Determination of the optical turbulence parameters from the adaptive optics telemetry: critical analysis and on-sky validation

Laurent Jolissaint,[1,*] Sam Ragland,[2] Julian Christou,[3] and Peter Wizinowich[3]

[1]*University of Applied Sciences Western Switzerland (HEIG-VD), 1, route de Cheseaux, CH-1401 Yverdon-les-Bains, Switzerland*
[2]*W. M. Keck Observatory, 65-1120 Mamalahoa Hwy., Kamuela, Hawaii 96743, USA*
[3]*Gemini Observatory, 670 No. A'ohoku Place, Hilo, Hawaii 96720, USA*
*Corresponding author: laurent.jolissaint@heig-vd.ch

It has been demonstrated by several authors that the optical turbulence parameters associated with a given adaptive optics (AO) run—the seeing angle and outer scale—can be determined from a statistical analysis of the commands of the system's deformable mirror (DM). The higher the accuracy on these parameters, the more we can make use of them, allowing for instance a better estimation of the seeing statistics at the telescope location or a more accurate assessment of the performance of the AO system. In the context of a point spread function reconstruction project (PSF-R) for the W. M. Keck observatory AO system, we decided to identify, in the most exhaustive way, all the sources of systematic and random errors affecting the determination of the seeing angle and outer scale from the DM telemetry, and find ways to compensate/mitigate these errors to keep them under 10%. The seeing estimated using our improved DM-seeing method was compared with more than 70 nearly simultaneous seeing measurements from open-loop PSFs on the same optical axis, and with independent seeing-monitor measurements acquired at the same time but far from the telescope (DIMM/MASS): the correlation with the open-loop PSF is very good (the error is about 10%), validating the DM-seeing method for accurate seeing determination, while it is weak and sometimes completely uncorrelated with the DIMM/MASS seeing monitor data. We concluded that DM-based seeing can be very accurate if all the error terms are considered in the DM data processing, but that seeing taken from non-collocated seeing monitors is of no use even when moderate accuracy is required.   © 2018 Optical Society of America

OCIS codes: (010.1290) Atmospheric optics; (010.1330) Atmospheric turbulence; (110.1080) Active or adaptive optics; (110.6770) Telescopes; (350.1260) Astronomical optics.

https://doi.org/10.1364/AO.57.007837

1. INTRODUCTION

We revisit in this paper the method to retrieve, from the commands of the deformable mirror (DM) of an adaptive optics (AO) system, two of the most important parameters of optical turbulence (OT): (1) the seeing angle, defined as the angular full-width-at-half-maximum (FWHM) of the seeing-limited long-exposure PSF and noted w_0 here, or equivalently the Fried parameter r_0; and (2) the optical outer scale, noted L_0. The method was introduced by Rigaut *et al.* [1], and has since been implemented by many other groups (see references), and we are using it in the context of a point spread function reconstruction (PSF-R) project for the W. M. Keck observatory AO system (a technique pioneered by Véran *et al.* [2]). The importance of a highly accurate seeing determination for PSF-R motivated the research described in this paper.

In the literature, the DM-based seeing monitor is mentioned as a particularly simple and efficient method for analysis such as AO system performance evaluation, assessment of the current seeing conditions, and PSF-R. Indeed, by using the AO data itself, it is possible to get an estimate of the seeing obtained *at* the telescope and *during* the observation—something not provided by seeing monitors because they are generally *not collocated* with the telescope, nor by measuring the seeing *before/after* the AO run, as the seeing changes too rapidly.

In the specific case of PSF-R, the seeing angle is critically needed to reconstruct the component of the PSF associated with the high spatial frequencies of the turbulent aberration (the DM *fitting error* in the AO jargon) located beyond the cutoff spatial frequency of the AO system, 1/(2 DM pitch). This error indeed dominates the residual wavefront in the case

of good seeing conditions, and is always significant in other cases.

Let us consider the case of the W. M. Keck 10 m telescope AO system (DM pitch 0.5625 m in the pupil), observing at $\lambda = 1.2$ µm with a seeing of $0.8''$. We find (not showing the details) that with a relative error of 10% on the seeing determination, the error on the Strehl is 10% as well. For a larger seeing angle, the error would be proportionally higher. For AO data processing (photometry, astrometry, deconvolution, etc.), this might be unacceptably large, knowing that the other PSF metrics errors, i.e., width or integrated energy, would be in the same proportions (see for instance Lu *et al.* [3]).

An accurate and simultaneous determination of the outer scale L_0 is also very important: because L_0 decreases the amplitude of the turbulent wavefront, it makes the angular size of a point-like object imaged through OT smaller than what it would be with a fully developed Kolmogorov turbulent flow. A small L_0 therefore has the same overall effect as a small seeing angle. Over- or underestimating the effect of the outer scale would produce an incorrect seeing angle estimation, with the consequences we have just seen. Note that there is no correlation between w_0 and L_0. Indeed, the widely used von Karman model is only an *empirical* method of correcting the infinite scales Kolmogorov model to account for the fact that there is *necessarily* an external limit to the size of the turbulent flow, with the consequence that the effect of the OT is always less severe than what is predicted by the Kolmogorov theory. For this reason in particular, the FWHM of an experimental long-exposure seeing-limited PSF will always be smaller than the w_0 predicted for a fully developed Kolmogorov flow.

Therefore, for the PSF-R project, we needed to identify as much as possible all sources of *systematic* and *random* errors on the seeing and the outer scale determination, known or unknown from the literature, and find ways to mitigate or suppress them. In this paper, we describe these errors and the way they are considered in our DM-seeing monitor algorithm, as well as the results of 841 AO testing runs from 2011 to 2017 in natural and laser guide star (NGS/LGS) modes. Our model considers in detail the following components of the problem in order of importance (Keck-II AO is a Shack–Hartmann wavefront sensor based system):

1. Choice of the pupil area to avoid the edges effect,
2. Impact of the central obscuration,
3. Zernike polynomial projection error and its mitigation by an adaptation of the polynomials to the DM influence function basis,
4. Zernike polynomial undersampling,
5. Deformable mirror influence function model,
6. Bad and good Zernike modes,
7. Contribution of the outer scale,
8. Wavefront sensor noise,
9. Shack–Hartmann wavefront sensor spatial aliasing,
10. Guide star mode, natural or laser.

Our seeing estimation method has been validated with a comparison of *almost* simultaneous seeing measurements from open-loop PSF. This is presented in the second part of this paper, where we also compare the DM-seeing results with simultaneous measurements from seeing monitors not collocated with the telescope, and show that the correlation is weak at best.

A. Previous Research

Our study complements a previous study by Schöck *et al.* [4], who used the same kind of method on the same telescope and AO system, but on open-loop wavefront sensor (WFS) data. Here, we use closed-loop DM data: this has the significant advantage that there is no need to open the loop to acquire the seeing data; therefore, the seeing estimation is absolutely simultaneous with the AO run, something mandatory for PSF-R.

Many authors have already used the DM-seeing method on several AO systems, essentially for AO system performance diagnostics during commissioning. Rigaut *et al.* [1] were probably the first to use the method for AO performance check, on the system COME-ON; Véran *et al.* [2] used the method in the context of the development of the first PSF-R algorithm, on the curvature-sensing-based AO system PUEO on the CFHT; Fusco *et al.* [5] have used the method on NAOS, the VLT first AO system, and did a first analysis of the error terms very similar to ours; the latter analysis was complemented by an analysis of the WFS aliasing effect by Kolb *et al.* [6].

Our own work considers the same terms as the previous authors, as well as additional terms which were not considered before. We have put a particular effort into the construction of a modal basis adapted to the telescope pupil, using a very accurate influence function empirical model, and to the selection of the modes actually used for the OT parameter estimation. Our outer-scale damping model has a larger domain of validity than previous models and is adapted to the scale of a 10 m telescope. In short, what makes this paper original is the emphasis put on details not considered before and the use of highly accurate models to account for complex effects. The large amount of sky data and the comparison with open-loop and seeing-monitor data allows us to clearly demonstrate the validity of the procedure and provide an estimation of the seeing determination accuracy.

2. DEFINITIONS

Let us recall the definitions of the OT quantities of interest in this study. For an introduction to OT theory, see Tatarski [7] and Roddier [8].

A. Seeing Angle

The seeing angle, noted as w_0, is defined as the FWHM of the long-exposure image of a point source seen through OT (ignoring diffraction from the telescope) when the turbulent flow is fully developed, i.e., the turbulent flow structure follows a Kolmogorov law, with infinite outer scale and null inner scale.

B. Fried Parameter

w_0 is related to the Fried parameter r_0 (Fried [9]), defined as the diameter of a telescope having the same optical resolution (integral of the OTF) as the long exposure optical resolution when looking through the aberrated optical system formed by OT. r_0 depends on the turbulence strength and the imaging wavelength λ, according to

$$r_0 = 1.6748 \left(\frac{\lambda}{2\pi} \right)^{6/5} \left[\int_0^\infty C_N^2(h) \mathrm{d}h \right]^{-3/5}, \quad \textbf{(1)}$$

where $C_N^2(h)$ is the vertical profile of the turbulent flow refractive index structure constant, a statistical second-order quantity similar to the refractive index variance. The seeing angle w_0 and the Fried parameter r_0 are directly related (Coulman [10]) to

$$w_0 = 0.98\lambda/r_0 \text{ [rad]}. \qquad (2)$$

Measurements of the seeing angle and the Fried parameter are therefore equivalent.

C. Optical Outer Scale

OT is a consequence of the turbulent mixing, due to the wind, of air masses at different temperature and hence different refractive index. Let us consider the typical difference $\Delta n = n(\mathbf{r} + \Delta\mathbf{r}) – n(\mathbf{r})$ of the refractive index between two points in the turbulent flow. Because of the turbulent mixing, the larger the separation, the higher the probability of experiencing large refractive index differences between the two points. If there is no upper limit to the extension of the turbulent flow, Δn will simply increase with Δr, and it is shown in Tatarski [7] that on average $\langle \Delta n^2 \rangle \sim \Delta r^{2/3}$.

Now, as there is necessarily an upper limit to the size of the largest eddies, the occurrence of large Δn is less probable when Δr increases beyond a certain limit, and $\langle \Delta n^2 \rangle$ saturates to a constant for large separations. The saturation distance is characterized by the so-called outer scale of optical turbulence L_0, related to the size of the largest eddies in the flow. Measurements in turbulent flow by many authors have clearly demonstrated the existence of this optical outer scale (see for instance Conan *et al.* [11] and Ziad *et al.* [12]).

As a consequence, the larger the telescope diameter with respect to L_0, the lower the wavefront RMS with respect to what we would expect for an infinite flow. Now, because r_0 is defined for an infinite flow, it is therefore mandatory, when using the DM-seeing method, to evaluate simultaneously the outer scale with the seeing angle in order to make an independent determination of the latter. Because a finite outer scale improves the image quality with respect to the infinite case, not taking into account L_0 would lead to overestimation of the Fried parameter, and underestimation of the seeing. The empirical outer-scale attenuation model we have developed for this purpose is described later in the text.

3. SUMMARY OF THE DM-SEEING METHOD

The AO system compensates the OT wavefront error by using the DM. As a consequence, at each instant, the DM surface (times 2, and introducing a cosine factor to take into account possible non-normal incidence) is naturally a good representation of the turbulent wavefront seen by the AO system up to its cutoff spatial frequency, with some perturbations due to the classical low-order AO errors, i.e., the servo-lag, WFS noise, and WFS aliasing. Therefore, from the DM command statistics, it must be possible to get an estimate of the average seeing associated with the AO observation. This idea has been validated in the context of PSF-R by Véran *et al.* [2], on the curvature wavefront-based AO system PUEO (Canada-France-Hawaii Telescope).

The Zernike polynomials basis is generally used for this purpose, and is also our choice here. A Karhunen Loeve basis could be considered too, but we would lose the benefit of having an analytical expression for both the polynomials and the optical

turbulence statistics (Noll distribution). It is a *modal* representation, as opposed to the DM influence function representation, which is *zonal*. The expression for the covariance of the Zernike coefficients z_k and z_l in the case of a pure Kolmogorov turbulent flow is given by Noll [13]. Winker [14] has supplemented Noll's model with the damping effect of the outer scale, and we have

$$\langle z_k z_l \rangle = (D/r_0)^{5/3} \mathcal{N}_{k,l} \mathcal{W}_{k,l}(D/L_0), \qquad (3)$$

where $\mathcal{N}_{k,l}$ is Noll's model and $\mathcal{W}_{k,l}$ is the L_0 damping factor from Winker. The OT parameters r_0 and L_0 can therefore be estimated by a best-fit adjustment of the preceding model to the measured covariances of the Zernike coefficients (this procedure is described in Section 7.A).

In AO systems, the DM commands are generally not expressed in the Zernike basis, but rather in a basis appropriate to the system's modes or in the DM influence function basis. In both cases, the Zernike covariance matrix is obtained from

$$\langle \mathbf{z} \cdot \mathbf{z}^t \rangle = \mathcal{M}_{az} \langle \mathbf{a} \cdot \mathbf{a}^t \rangle \mathcal{M}_{az}^t, \qquad (4)$$

where t indicates transposition, $\mathcal{M}_{az}$ is the transformation matrix from the DM basis to the Zernike basis, and $\langle \mathbf{a}\mathbf{a}^t \rangle$ is the DM command covariance matrix. In this notation, we assume that $\mathbf{a}$ and $\mathbf{z}$ are column vectors. The OT parameters are in principle estimated by adjusting Eq. (3) to the measured covariance matrix computed from Eq. (4).

As given, however, this model cannot be used because many effects (listed in the introduction) generating systematic and random errors affecting the DM commands and the Zernike basis construction have not been considered. The objective of this paper is specifically to address all these errors terms, and show how they can be compensated.

4. CONSTRUCTION OF A MODAL BASIS, CONSIDERING THE PUPIL EDGES AND THE DM ZONAL MODES

In this section, we show how the classical Zernike modal basis, as defined by Noll [13], and the coefficients covariance model $\mathcal{N}_{k,l}$ are modified to suppress or minimize the impact of the following effects: the pupil edge, the central obscuration, the Zernike projection error and Zernike under-sampling, the DM influence functions model, and the bad modes.

A. Pupil Edge Effects

In an AO system, actuators whose influence functions are partially outside of the *external* pupil edge have to be given a larger command than the ones that are fully illuminated. Indeed, those actuators, if given a command amplitude identical to the illuminated ones, generate a DM surface that is too low in amplitude because at this location there are less actuators whose influence functions can overlap. Indeed, the total surface amplitude of a set of (for instance) 3-by-3 neighbor actuators is higher than a single actuator receiving the same command, because the wings of the 3-by-3 influence functions add together and lift the DM surface to a higher amplitude. To compensate for the lack of amplitude inside the pupil, on the edge, the AO control simply gives a higher command to the corresponding actuators.

Other issues affect the actuator commands, on the pupil external edge as well as inside the central obscuration: at this
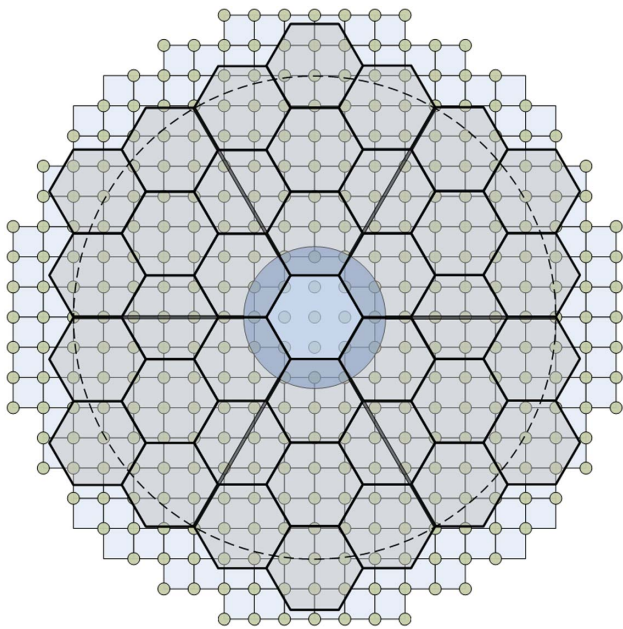
Fig. 1. Keck telescope segmented pupil, with a superposition of the DM actuator and SH-WFS lenslet layout. The blue disc is 2.65 m in diameter and shows the central obscuration. The dashed circle shows the 9 m diameter of the pupil area within which the lenslets are always fully illuminated, independently of the pupil/DM angle. Note that this overlay shows only one possible orientation of the telescope pupil relative to the AO system. Courtesy W. M. Keck Observatory.

location, at least in the case of a SH-WFS, the lenslets are vignetted, generating a systematic error as well as a random error on the wavefront measurement due to the lower signal-to-noise ratio. On top of this, in the specific case of the Keck hexagonal pupil, because the latter rotates with respect to the lenslet array, the vignetting changes during the exposure, as we understand from Fig. 1.

All these effects make the DM surface statistics not stationary along the pupil external/internal edges. Figure 2 shows the standard deviation of the DM surface of the Keck-II AO system for one of our on-sky PSF-R experiments. It is constructed as the RMS value of the DM surface at each DM points for 35,912 loop sequences at a frame rate of 1 kHz. We can see that the surface deviation is 2–4 time larger, on the external edges of the DM as well as inside the central obscuration, than inside the fully illuminated pupil.

Now, with the DM seeing monitor technique we are using, it is assumed that the turbulent wavefront *is* stationary, within a *circular* pupil. So, to avoid overestimating the turbulent wavefront RMS and the seeing angle, and to have a circular pupil (in the specific case of Keck), we must limit the seeing estimation within a smaller annular section on the telescope pupil where the DM commands can be considered stationary.

Figure 1, for Keck, shows the circular area on the 36-segment pupil which is always illuminated regardless of the pupil orientation with respect to the WFS lenslet array. It is therefore clear that this limit (9 m in diameter) is a good choice to define the pupil for the seeing computation (the telescope central obscuration is 2.65 m). Figure 2 clearly shows that the DM
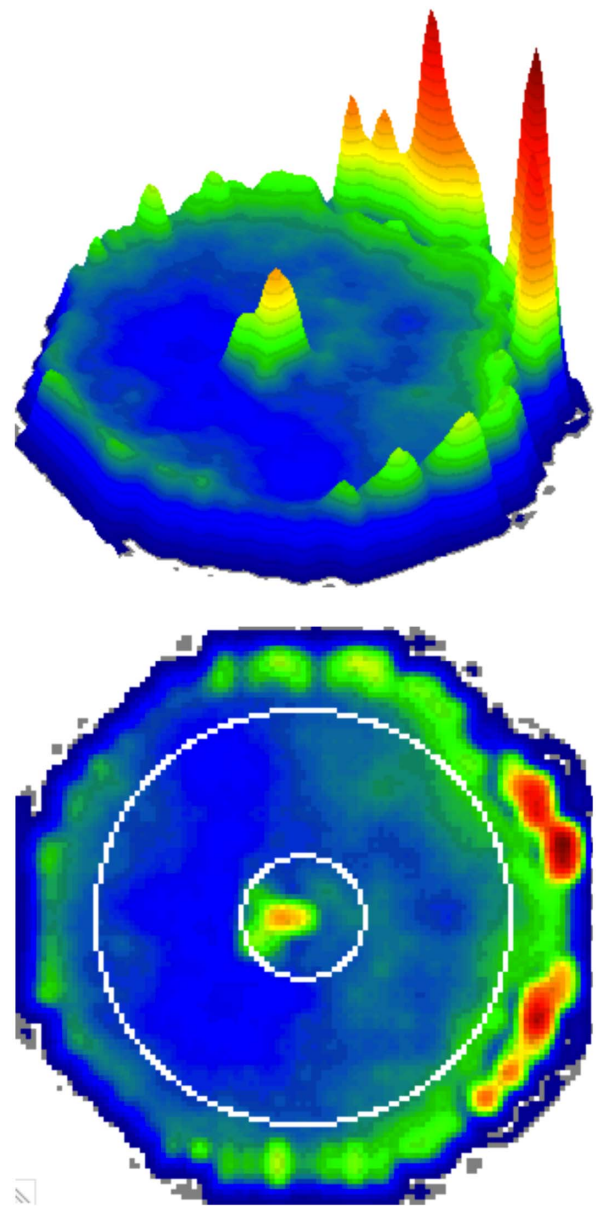

Fig. 2. RMS map of the DM wavefront for a typical AO run, over 35,912 loop sequences at 1 kHz. The spatial resolution is 7 pixels per DM pitch length. The white circles show the limits of the 2.65 m and 9 m diameter annular pupil.

surface is stationary within this 9/2.65 m pupil (white circles), at least relative to the edges.

In practice, to decide on the pupil diameter for the seeing estimation, we can compute how stationary the DM surface RMS is when averaged over an annulus of increased external radius, from the central obscuration to the telescope pupil radius. We did this with the Keck pupil for a radius from a little more than the central obscuration radius up to the maximum telescope *hexagonal* pupil radius, 6.2 m. The result, for 79 AO runs, is shown in Fig. 3.

As we can see, there is some level of non-stationarity in the fully illuminated area (otherwise the RMS of the DM wavefront RMS would be 0), but this is in general relatively stable
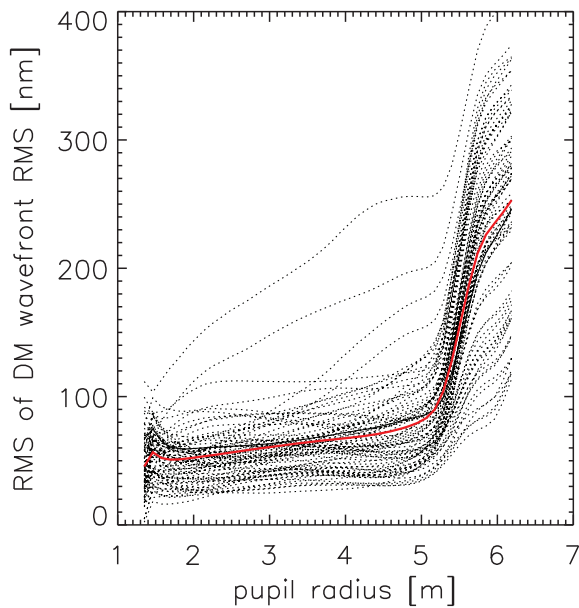
Fig. 3. Stationarity of the DM wavefront as a function of the pupil radius. The dotted curves show each of the 79 cases for the night of August 1, 2013. The red curve shows the average of all cases.

until the average hexagonal pupil radius is reached near 5 m. Beyond, the non-stationarity increases very strongly. It therefore seems very reasonable to consider the pupil 9/2.56 meters for the seeing estimation.

Note that the secondary support structure arms are very thin (2.54 cm) in the case of the Keck telescopes, and therefore we do not take this structure into account in the pupil model. Only the very high-order Zernike polynomials (radial order 600) would be affected at this spatial scale.

B. Modified Zernike Basis

The DM commands are applied to the actuators, so the actual DM surface shape belongs to the space defined by the actuators' influence function basis. Noll's model, on the other hand, is given in the Zernike basis, so a change of basis is required which is very simple to do, numerically, using an orthogonal projection of the Zernike basis into the influence functions basis. However, this procedure introduces systematic errors.

First, the Zernike polynomials are *not* well represented by the influence function basis. The difference between a Zernike polynomial and its projection on the DM basis can be significant, more than a few percent, and varies in a complicated way with the Zernike index j and azimuthal order m, as Fig. 4 shows. This would generate a *systematic* error in the estimation of the variances of the DM commands expressed in the Zernike basis simply because the transformation matrix does not generate the true Zernike coefficients.

The second difficulty comes from the limited numerical sampling of the influence functions and Zernike polynomials while computing the DM to Zernike transformation matrices. This error term is shown by the black curves in Fig. 4. Thus, even without the projection error, the limited numerical sampling already induces a systematic error of a few percent, strongly depending on the Zernike index.
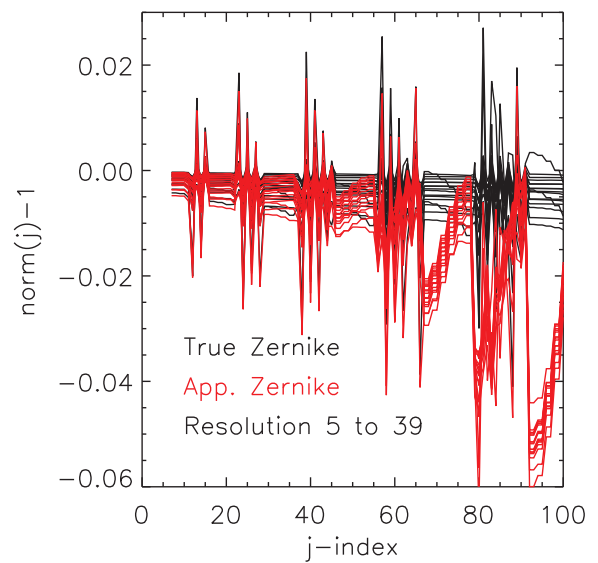

Fig. 4. Effect of the projection and numerical sampling errors on the Zernike polynomial norm (here −1), up to $j = 100$. The black lines show the difference between the norm computed numerically on the true Zernike polynomials and the theoretical value (which is 1). The different lines are for increased numerical resolution, defined as the number of pixels per actuator pitch. The higher the resolution, the smaller the error, in principle. There are 16 actuator pitches across the pupil in this example. The red lines show the same, but for the Zernike polynomial projection in the DM influence function basis. There is no central obscuration in this example.

The third source of error comes from neglecting the central obscuration. When it is relatively large (say, more than 10% of the pupil diameter), the central hole significantly changes the norm of some Zernike polynomials and generates, if not taken into account, a systematic error in the coefficient variances, as illustrated in Fig. 5.

The solution to these systematic errors is simple: orthogonality of the modes that we use to express the OT wavefront error is *not* required—independence of the modes is indeed sufficient—so we can simply consider, as a modal basis, the projection of the Zernike polynomials on the influence functions basis, including the central obscuration. The sampling error can be minimized by using the highest sampling resolution compatible with a reasonable computation time. We shall call these polynomials the *modified Zernike polynomials*, noted $\widehat{Z}_j$. They differ from the true Zernike by a term e_j,

$$Z_j = \widehat{Z}_j + e_j = \sum_{i=1}^{N_a} \hat{a}_{j,i} A_i + e_j, \qquad (5)$$

where A_i are the actuator's influence functions and $\hat{a}_{j,i}$ the coefficients of each modified Zernike in the actuator's basis. With this new basis, if we have enough modes $\widehat{Z}_j$, any DM shape φ_{DM} can be represented without numerical error and the equality below becomes exact:

$$\varphi_{DM} = \sum_{j=1}^{N_z} \hat{z}_j \widehat{Z}_j. \qquad (6)$$

The concatenated column vectors $\hat{\mathbf{a}}_j$, made from the coefficients $\hat{a}_{j,i}$ in Eq. (5), generate the matrix $\mathcal{M}_{az}$ to compute the
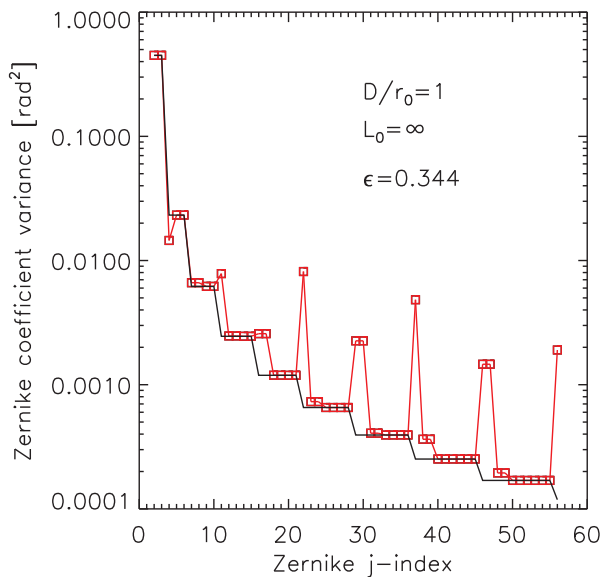
Fig. 5. Zernike coefficient variances when including a central obscuration of 34% in the pupil. The example is voluntarily extreme to show the effect on the polynomials for which $m = 0$ and $m = 1$. There is no DM projection error here. See also Fig. 1 of Véran *et al.* [2], showing the strong effect of the large central obscuration of the CFH telescope.

modified Zernike from the influence functions. Its dimension is N_a lines and N_z columns. They are calculated numerically with the classical orthogonal projection of the true Zernike into the DM actuator basis,

$$\text{for each } \widehat{Z}_j \quad \hat{\mathbf{a}}_j = \Gamma^{-1}\mathbf{b}_j, \tag{7}$$

$$\text{where } \begin{cases} b_{j,i} = \iint_P \widehat{Z}_j A_i \mathrm{d}^2 r \\ \Gamma_{k,l} = \iint_P A_k A_l \mathrm{d}^2 r \end{cases}, \tag{8}$$

and the integration is computed inside the annular pupil P.

1. Realistic Empirical Model for the DM Influence Function
In order not to add another source of systematic error to the seeing estimation, it is clear that the influence function model to use in the preceding basis transformation has to be as realistic as possible; otherwise it would make no sense to consider the projection error, as it depends on the influence function shape. For the Keck AO DM, Gaussian, double-Gaussian, or/and Moffat profiles are not accurate enough because they do not capture the variation of the influence function section shape, from square (bottom) to circular (top).

We had access to accurate interferometric measurements of the influence functions of the Gemini North AO system DM (Altair), made from the same technology and produced by the same manufacturer as Keck's DM (Xinetics, Inc.) From these measurements, we have built a high-fidelity empirical model, reproducing the influence function section shape at all heights.

Our model, $\mathcal{I}(x, y)$, is given below and is represented in Fig. 6. The unit of the coordinate $(\mathbf{x}, \mathbf{y})$ is pitch length. It is essentially a negative exponential model, with an adjustment
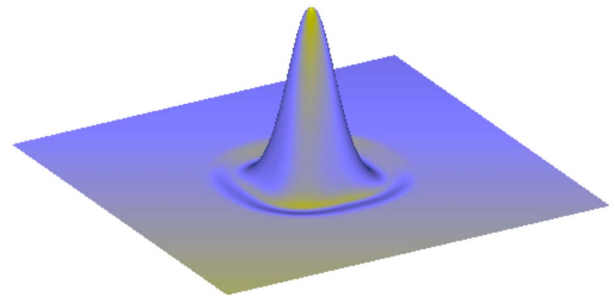

Fig. 6. Empirical model of the Xinetics Inc. deformable mirror influence function.

to account for the negative drop at the foot of the influence function, in which the section of the influence function varies gradually from a circle at its top to a square with round edges on its bottom (modeled with the functions ρ and ϵ). There is an overall mask function $\mathcal{M}$ to strongly but smoothly cut the edge of the influence function to limit its extension over the DM:

$$\mathcal{I}(x, y) = \exp(-p_4\rho)(1 + p_5\rho)\mathcal{M},$$
$$\rho = p_6^\epsilon(|x|^\epsilon + |y|^\epsilon),$$
$$\epsilon = (p_0 + p_1 r^2 + p_2 r^4 + p_3 r^6)\mathcal{M},$$
$$\mathcal{M} = \exp(-p_7 r^8), \tag{9}$$

where $r^2 = x^2 + y^2$, and the eight parameters p_i are given as

$$p_{0...7} = \begin{bmatrix} 2.24506 \\ 2.042278 \times 10^{-1} \\ -1.921478 \times 10^{-2} \\ 1.070762 \times 10^{-3} \\ 7.693368 \times 10^{1} \\ -3.979560 \times 10^{1} \\ 1.802674 \times 10^{-1} \\ 1.672743 \times 10^{-4} \end{bmatrix}.$$

Our model follows the measured influence function with an error of less than 1% over the full influence function footprint. Therefore, it will not be a significant source of error.

C. Constructing the Modified Zernike Basis Coefficient Variance Model for Kolmogorov Turbulence

Of course, with the Zernike basis modification, *we cannot* use Noll's covariance model anymore, and it has to be recomputed. This is easily done with a Monte Carlo simulation of a large number of independent turbulent phase screens (10,000 screens allows for 1% convergence) with $D/r_0 = 1$ and $L_0 = \infty$, projected orthogonally on the modified Zernike basis. From the resulting series of modified Zernike coefficients, the covariances are directly computed. Note that we assume that Winker's correction factor is only marginally affected by the systematic errors indicated previously, so only the term $\mathcal{N}_{k,l}$ is modified. Indeed, an exact calculation of the correction factors would require us to use the modified Zernike polynomials, but this would only change the Zernike variances from Winker's model by the same amount that we have seen above for Noll's variance, i.e., a few percent. In other words, we would change

the *correction* factor by a few percent, and the effect would therefore be minimal. Therefore, we have decided not to recompute Winker's model.

D. How Many Modes Should Be Considered and Which Ones Should Be Avoided?

The higher the Zernike polynomial index, the higher the spatial frequencies within the polynomial. Now, beyond some j-index, the oscillation period in the radial and azimuthal components of the polynomial will be much shorter than the influence function spatial extension, and the projection coefficient $b_{j,i}$ in Eq. (8) will gradually drops to zero.

For the Keck system, using our influence function model, we have found that above $j = 2000$, the projection coefficient $b_{j,i}$ becomes negligible and the DM is no longer sensitive to these polynomials. But in the Keck case, as we will see, the Zernike polynomial sampling error just introduced affects the variance model for j-indexes much lower than $j = 2000$.

Besides, there is no need to use such a large number of modes; indeed, a few hundred is enough to get an excellent adjustment of the modified Noll–Winker variance model. And finally, it is intuitive that for the high-order modes, the impact of the wavefront sensing noise can only increase. In the end, only a careful examination of the signal-to-noise ratio of the AO system considered and the effect of the numerical undersampling can tell what must be the maximum number of modes to use.

Finally, the modes susceptible of being affected by *non-turbulent* sources of aberrations—the bad modes—must be excluded from the seeing computation because their coefficients will carry an *excess* of variance relative to the turbulent variance. Sources of dynamic non-turbulent errors are generally the wind-induced telescope jitter, telescope tracking errors, and mirror wrapping in the case of large or segmented primary mirrors generating astigmatism, defocus, and possibly some coma. These instrumental aberrations are low order, and are practically null at orders higher than, generally, spherical aberration (fourth radial order). This excess of low-order variance would be interpreted as a larger outer scale than the actual value, and as we are correcting the Zernike variances for the damping effect of the outer scale in order to get an estimation of the Fried parameter, sub-correcting would lead to an underestimation of w_0. Of course, only a quantitative estimation of the instrumental variance for each mode can tell which are the modes to avoid, but clearly at least tip-tilt must be excluded.

E. Modified Zernike Coefficients Variance in Practice: The Case of Keck AO

We have applied the Monte Carlo method just described to the Keck AO system influence function basis and pupil. Figure 7 shows the variance of the modified Zernike coefficients for a turbulence $D/r_0 = 1$, an infinite outer scale, a central obscuration $\epsilon = 2.65/9 = 0.294$, and a resolution of 29 pixels per actuator pitch.

As said previously, we exclude tip-tilt from the basis, but also the defocus and the two astigmatisms: indeed, even if we are not certain that the Keck telescope optical system generates these second-order aberrations, these are very often seen in other systems, so we prudently prefer to discard them. To give
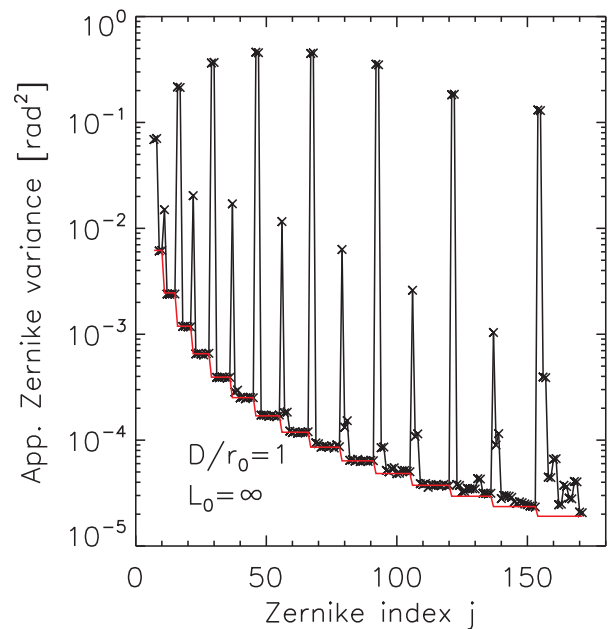

Fig. 7. Modified Zernike mode coefficient variances for the 9/2.65 m Keck annular pupil, for a $D/r_0 = 1$ and an infinite outer scale. The red line shows the true and unobstructed Zernike mode variances computed from Noll [13].

an order of magnitude of the impact of an excess of defocus and astigmatism, we ran our seeing and outer-scale estimation method on a simulated distribution of Zernike variances for a seeing of 1″ and an outer scale of 13 m (close to the average value we found for the telescope). If each of the Z_4, Z_5, and Z_6 have an extra instrumental error of 100 nm RMS, the seeing angle is overestimated by 2%. If we double the instrumentation error, the seeing angle overestimation is 4%. The effect is not enormous, but it can be easily avoided by unselecting these potentially instrumental-error-sensitive aberrations.

The first modified Zernike modes we are therefore considering in the model are the two comas Z_7 and Z_8, and the last are the ones associated with the radial order $n = 17$, corresponding to Z_{171}. The effect of the central obscuration is well apparent: for the azimuthal orders $m = 0$ and $m = 1$, the modal variance is several orders of magnitude higher than Noll's model, showing *a posteriori* the importance of considering this parameter. For most modes, though, the variance is close to Noll's model.

In the same figure, we can also see that beyond the index $j = 153$, corresponding to the last polynomial of radial order $n = 16$, the departure with Noll's variance becomes erratic. Because this is not the case for the previous modes, we think this is a consequence of the numerical undersampling error. We decided therefore to limit the Zernike index range from 7 to 153 (radial orders 3 to 16), which still makes 147 good modes.

5. OUTER-SCALE VARIANCE ATTENUATION MODEL

We now need a model for $\mathcal{W}_{k,l}$, the damping factor of the modal variances due to the optical outer scale.
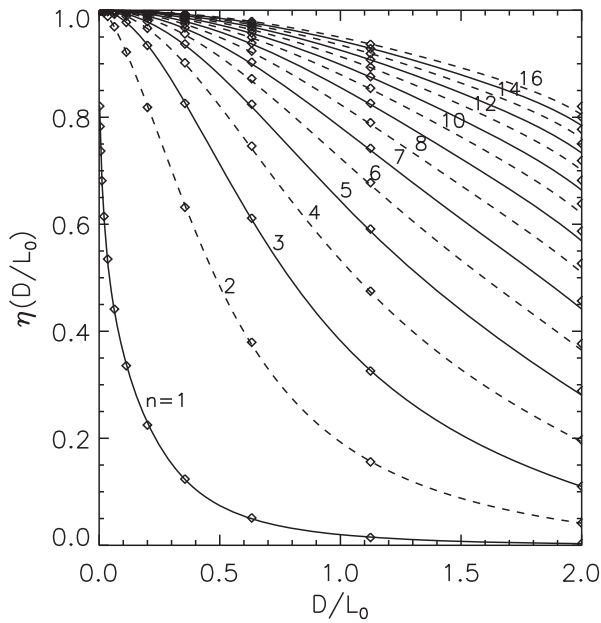
Fig. 8. Damping of the Zernike coefficient variances as a function of D/L_0 and radial order n. Diamonds show the exact computation of the damping factor (courtesy D. Winker), and the cont/dashed lines are our empirical model.

Winker [14] has developed the analytical expressions for the covariance of the Zernike coefficients, in a Von Karman model of the optical turbulence phase spatial power spectrum, as a function of D/L_0. These equations contain hypergeometric functions which are not practical to handle in a minimization algorithm such as ours. Also, we only need a model for the variances of the Zernike coefficients, not the covariances, so in our case $k = l$.

Winker provided us with a grid of $\mathcal{W}_{j,j}$ values for a range $D/L_0 = [0.002, 2]$ (or $L_0/D = [0.5, 500]$) and Zernike indexes up to $j = 153$ (or $n = 16$), and from these data we have built an empiric model of the damping factor (see Fig. 8). In its domain of validity, the accuracy of our model is about 1%.

Defining $x \equiv D/L_0$, with n being the radial order associated with the Zernike index j, the model is given by

$$\mathcal{W}_{j,j}(x) = \frac{\exp\{-n^{[A(x)\ln n + B(x)]} \exp C(x)\}}{1 + 13.6334(x/n)^2}, \quad \textbf{(10)}$$

where

$$A(x) = \sum_{i=0}^{5} \alpha_i \ln^i(x),$$

$$B(x) = \sum_{i=0}^{5} \beta_i \ln^i(x),$$

$$C(x) = \sum_{i=0}^{5} \gamma_i \ln^i(x), \quad \textbf{(11)}$$

and the coefficients α_i, β_i, and γ_i are given in Table 1.

Figure 9 shows the variance attenuation expected for a 9 m pupil and an outer scale of 13 m, equal to the average of what we have measured on the Keck telescope (see Section 7). It can

Table 1. Coefficients of the L_0 Variance Attenuation Model

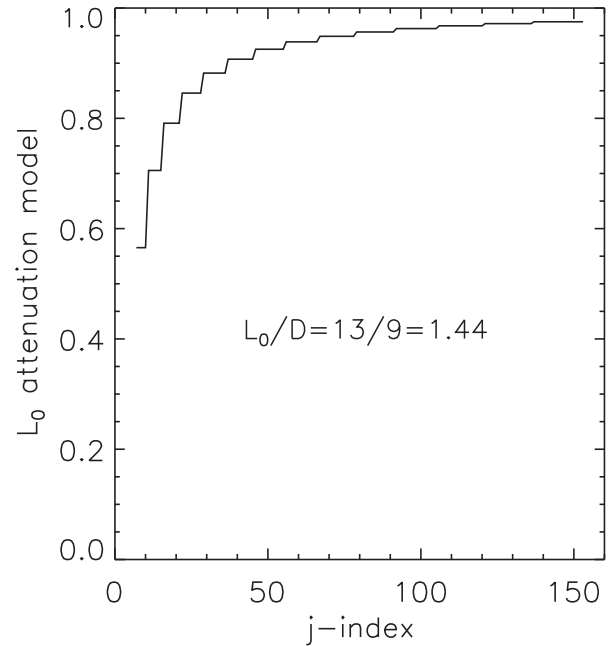| $\alpha_{0...5}$	$\beta_{0...5}$	$\gamma_{0...5}$
−0.54628	−2.55240	0.21361
0.76701	0.36600	0.27999
0.27252	0.45688	0.28100
0.05060	0.36283	0.14758
0.01861	0.05929	0.02611
0.00191	0.00310	0.00156

Fig. 9. Expected variance attenuation for the 9 m Keck telescope seeing estimation pupil considering an outer scale of 13 m, equal to the average value measured using the DM seeing monitor.

be seen that when the outer scale is on the order of the pupil diameter, its effect on the variance is very significant even on the highest radial orders.

6. PREPARATION OF THE DM DATA

The DM commands m_k are built from the application of the command matrix to the WFS measurements vector, followed by the application of a control law (at the minimum a simple integrator). For a well adjusted and aligned system, the sources of WFS measurement error are essentially the detector and photon noise, and the WFS spatial aliasing of the high-frequency part of the turbulent wavefront. These errors are added to the DM commands during reconstruction and control.

It is relatively easy to build a model of the covariances associated with these two errors terms, allowing us to identify and remove them from the DM command statistics. This procedure was first described by Véran et al. [2] for a modal system and a curvature WFS. Here it is adapted to the Keck AO, a zonal and Shack–Hartmann WFS based system.

Assuming that the AO system does not suffer from significant calibration and alignment errors, the command m_k to actuator k, at each loop instant, is given by the sum of the following components:

$$m_k = a_{\parallel,k} + n_k + a_{\parallel,k}^{\perp}, \tag{12}$$

where $a_{\parallel,k}$ is the projection coefficient on the kth influence function of the low-frequency part of the turbulent wavefront that can be seen by the WFS, averaged over the WFS integration time and delayed by the data processing time required by the loop operations; n_k is the random command noise associated with the WFS noise; and $a_{\parallel,k}^{\perp}$ is the command error due to the WFS spatial aliasing of the high spatial frequencies into the low-frequency domain.

The covariance of the coefficients $a_{\parallel,k}$ is what is needed in Eq. (4) to compute the modified Zernike coefficients covariance, on which the modified Noll–Winker model is applied. It is given by

$$\langle \mathbf{a}_{\parallel} \cdot \mathbf{a}_{\parallel}^t \rangle = \langle \mathbf{m} \cdot \mathbf{m}^t \rangle - \langle \mathbf{n} \cdot \mathbf{n}^t \rangle$$
$$- \langle \mathbf{a}_{\parallel}^{\perp} \cdot \mathbf{a}_{\parallel}^{\perp t} \rangle - \langle \mathbf{a}_{\parallel} \cdot \mathbf{a}_{\parallel}^{\perp t} \rangle - \langle \mathbf{a}_{\parallel}^{\perp} \cdot \mathbf{a}_{\parallel}^{t} \rangle. \tag{13}$$

The first term on the right member dominates the others, except in the case of a faint guide star. The noise is correlated between neighbor actuators sharing the same area of the WFS, so its covariance matrix is not diagonal. But the noise is not correlated with the atmospheric signal, and therefore covariance between $\mathbf{n}$ and $\mathbf{a}$ is null.

Let us discuss first how to evaluate the noise covariance from the DM commands themselves. We will discuss the estimation and compensation of the aliasing contribution next.

A. Compensating for the Wavefront Sensor Noise

We are aware of two methods to evaluate the noise level. The first involves a statistical modeling of the WFS signal: comparing the real statistics with the expected statistics in the absence of noise, the noise variance can be estimated. This powerful technique has been developed by Véran *et al.* [2] and tested on a curvature-sensing WFS. An adaptation to the Shack–Hartmann WFS is given in Jolissaint *et al.* [15]. This technique requires the raw WFS data (the WFS camera pixel values). We did not get access to these data in the Keck experiment, so we had to turn to the second technique: the noise power spectrum method, detailed in the following.

1. Estimating the WFS Noise Variance Using the Noise Transfer Function

Figure 10 shows the temporal power spectrum (t-PSD) of the command to one of the actuators of the Keck AO system DM. At low frequency, the spectrum is dominated by the atmospheric signal. At high frequency, the spectrum saturates to a noise plateau. As the noise transfer function can be computed from the parameters of the AO loop, which are known by design, it is possible to adjust to the data a model of the filtered t-PSD of the two components $\mathbf{m}$ and $\mathbf{n}$, and extract the noise variance from the fit (the procedure to go from the noise t-PSD to the noise variance will be detailed later).

Let us develop the DM commands t-PSD model. The AO loop diagram is shown in Fig. 11. $\mathbf{a}_{\parallel}$ indicates the vector of the projection of the turbulent phase into the DM mode basis
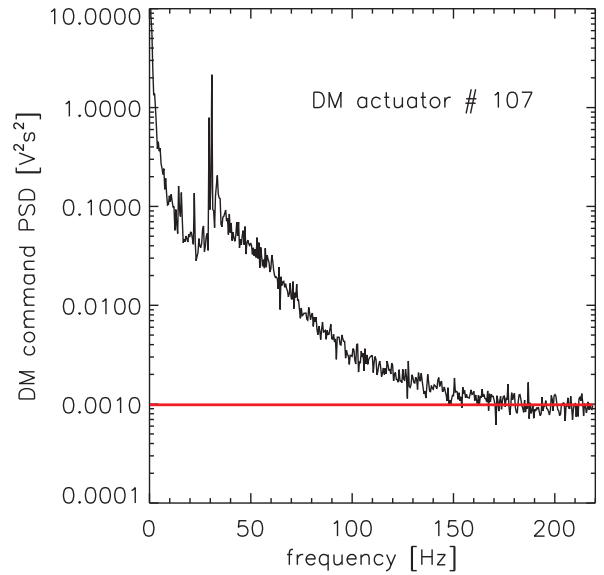

Fig. 10. Temporal PSD of the command to the actuator # 107. The red line shows the convergence to the white noise plateau. With a guide star magnitude 11 in R-band for this example, the signal noise is moderate. The t-PSD has been smoothed in this figure.

(any of the actuators), and $\mathbf{e}$ is the residual after partial correction by the DM command $\mathbf{m}$, i.e., $\mathbf{e} = \mathbf{a}_{\parallel} - \mathbf{m}$. The model is developed in the continuous frequency domain (ν [Hz]), and hence the Laplace transform is used. Once the AO system is running, the transient response is quickly over, and therefore the argument of the Laplace transform can be replaced with $s = i2\pi\nu$.

With ν_s standing for the loop sampling frequency, the transfer functions of each block are as follows:

1. The WFS transfer function is the composition of a time average and a time shift (half a loop period):

$$W(\nu) = \text{sinc}(\nu/\nu_s) \exp(-i\pi\nu/\nu_s). \tag{14}$$

2. The WFS aliasing transfer function is the same as the WFS transfer function; it is only the shape of the aliased signal power spectrum that differs from $a_{\parallel}$.

3. The time delay transfer functions for the WFS detector reading, wavefront reconstruction, and command computation are all given by the same equation,

$$R(\nu) = \exp(-2\pi i \Delta t \nu), \tag{15}$$

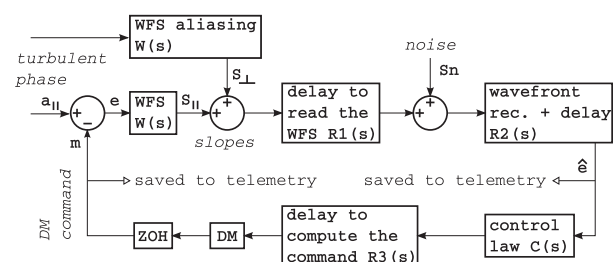where Δt is the time delay.

Fig. 11. Block diagram of the classical Keck AO system, based on a single Shack–Hartmann wavefront sensor.

4. The control law transfer function for the Keck AO control system, based on a third-order proportional, derivative and integration (PID) algorithm, is given in the discrete domain by (see van Dam *et al.* [16]):

$$C(z) = \frac{a_0 + a_1 z^{-1} + a_2 z^{-2} + a_3 z^{-3}}{1 + b_1 z^{-1} + b_2 z^{-2} + b_3 z^{-3}}, \quad (16)$$

where the Z-transform argument z is replaced by $\exp i2\pi\nu/\nu_s$ when we want to express this law in the continuous domain. The coefficients a_i and b_i are set by design. a_0 is the proportional loop gain, and b_1 is set to a value slightly smaller than 1 (leaky integrator gain) in order to avoid invisible modes building up in the DM commands. Note that the control law might vary between systems. Our objective here is only to demonstrate the noise-reduction technique on a particular case, the Keck AO system.

5. The DM transfer function is assumed to be 1, as the first mechanical resonance frequency is much higher than the usual bandwidth of the AO system.

6. The zero-order hold transfer function is actually 1 because it is already included in the WFS integration time.

From inspection of the loop diagram in Fig. 11, we find, for the amplitude spectrum of the command of actuator k (we skip the frequency in the notation to improve the reading and ~ indicates a Fourier transform),

$$\tilde{m}_k = H_{CL}\tilde{a}_{\parallel,k} + \frac{H_{CL}}{W R_1} \widetilde{wn}_k, \quad (17)$$

where the aliasing term is ignored (we will take care of its contribution in the direct space, not using the current transfer function method). Here,

- wn_k is the kth component of the transformation of the slope white noise vector $\mathbf{S}_n$ into a white noise actuator command vector (by application of the command matrix D^+), and is related to the noise command n_k we are interested in Eq. (12) by

$$\tilde{n}_k = \frac{H_{CL}}{W R_1} \widetilde{wn}_k. \quad (18)$$

- H_{CL} is the closed-loop transfer function,

$$H_{CL} = \frac{W R_1 R_2 R_3 C}{1 + W R_1 R_2 R_3 C}. \quad (19)$$

- $\tilde{a}_{\parallel,k}$ is the spectrum of the turbulent phase projected onto actuator k.

From Eq. (17), we can now compute the cross-spectrum of the DM commands (⋆ indicates complex conjugation),

$$\tilde{m}_k \tilde{m}_l^\star = |H_{CL}|^2 \tilde{a}_{\parallel,k}\tilde{a}_{\parallel,l}^\star + \frac{|H_{CL}|^2}{W R_1}(\tilde{a}_{\parallel,k}\widetilde{wn}_l^\star + \tilde{a}_{\parallel,l}^\star\widetilde{wn}_k)$$
$$+ \left|\frac{H_{CL}}{W R_1}\right|^2 \widetilde{wn}_k\widetilde{wn}_l^\star. \quad (20)$$

The second term of the right member of the equation is null on average, and does not contribute to the t-PSD. The model of the temporal cross spectrum that we need to fit to the data, considering that $|R_1| = 1$, is therefore

$$\langle \tilde{m}_k \tilde{m}_l^\star \rangle = |H_{CL}|^2 \langle \tilde{a}_{\parallel,k}\tilde{a}_{\parallel,l}^\star \rangle + \left|\frac{H_{CL}}{W}\right|^2 \langle \widetilde{wn}_k\widetilde{wn}_l^\star \rangle. \quad (21)$$

Practically, the procedure to get the white noise covariance $\langle \widetilde{wn}_k\widetilde{wn}_l^\star \rangle$ is the following:

1. From the telemetry, compute the actuator command temporal power cross-spectrum $\langle \tilde{m}_k \tilde{m}_l^\star \rangle$;

2. Build the closed loop and WFS transfer functions;

3. Multiply the commands cross-spectrum with the ratio $|W/H_{CL}|^2$ to make the high-frequency $\widetilde{wn}_k\widetilde{wn}_l^\star$ white noise cross-spectrum plateau evident;

4. At this point, we are left with a temporal cross-spectrum term equal to

$$\langle \tilde{a}_{\parallel,k}\tilde{a}_{\parallel,l}^\star \rangle|W|^2 + \langle \widetilde{wn}_k\widetilde{wn}_l^\star \rangle. \quad (22)$$

Here, there are two options: either we have some clue about the atmospheric signal, in which case we can adjust a model to the spectrums $\tilde{a}_{\parallel,i}$; or we do not, in which case (a) we use the fact that the atmospheric signal is low at high frequency and is dominated by noise, which is generally true unless we work at very low sampling frequency, and (b) we evaluate the average level of the high-frequency plateau (Fig. 12). This is actually the easiest way. Indeed, knowing the atmospheric signal would actually require us to know not only the seeing, but also the vertical distribution of the turbulence and wind velocity. In this case, we would not need the DM-based seeing monitor.

Therefore, we have no choice but to assume that the noise dominates the signal at high frequency, and make a reasonable choice of the frequency above which the average of the t-PSD plateau is computed. Of course, it is possible to iterate: get a first estimate of the seeing, assume a certain vertical distribution of the OT and wind profiles, compute the terms $\tilde{a}_{\parallel,k}$, and redo the estimation. Due to the large number of assumptions that are needed in such a case, it remains to be demonstrated that this iterative procedure brings any advantage.

5. Once the white noise t-PSD plateau level $\langle \widetilde{wn}_k\widetilde{wn}_l^\star \rangle$ is estimated, the command noise covariance can be computed using Parseval equality:
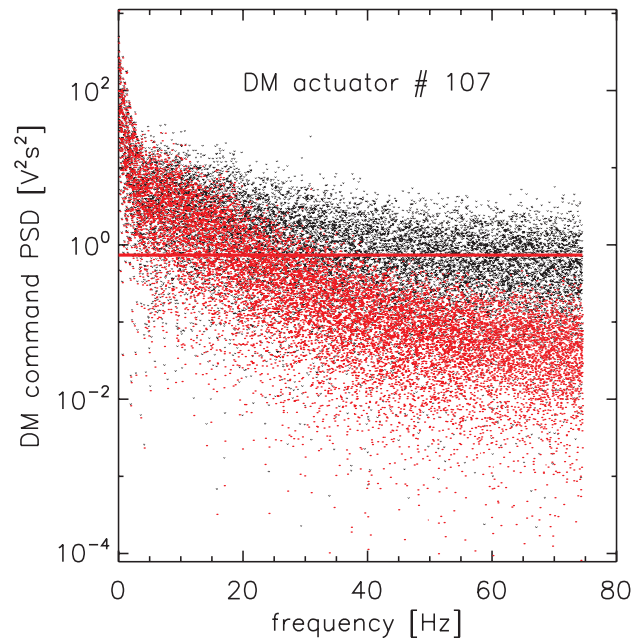

Fig. 12. Red dots show raw DM command t-PSD for actuator # 107. Guide star magnitude 14.5 (R-band). Black dots: after compensating with the transfer function $|W/H_{CL}|^2$. The red line shows the estimated white noise t-PSD level.
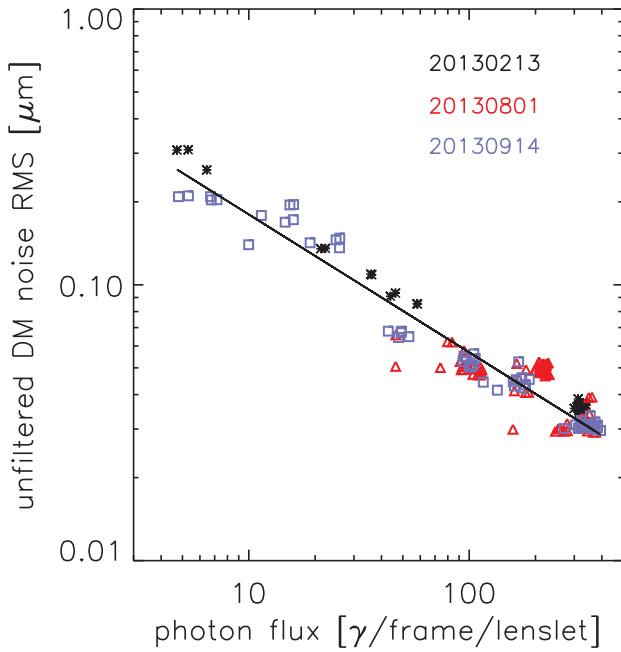
Fig. 13. Unfiltered DM command white noise RMS as a function of the number of photons N_γ per WFS integration time, for actuator number 107. The line shows the expected behavior in $1/\sqrt{N_\gamma}$.

$$\langle n_k n_l \rangle \equiv \frac{1}{T} \int_t n_k(t) n_l(t) \mathrm{d}t = \frac{1}{T} \int_\nu \tilde{n}_k(\nu) \tilde{n}_l^\star(\nu) \mathrm{d}\nu$$

$$= \langle \widetilde{wn}_k \widetilde{wn}_l^\star \rangle \int_\nu \left| \frac{H_{CL}(\nu)}{W(\nu)} \right|^2 \mathrm{d}\nu. \qquad (23)$$

This procedure is illustrated in Fig. 12 on the power spectrum ($k = l$) of a noisy signal. The white noise plateau is well apparent. We also compare in Fig. 13 the estimated actuator noise as a function of the number of photoelectrons detected during the WFS integration over the full detector, with the theoretical law in $1/\sqrt{N_\gamma}$. This is done for about 100 data sets, over three nights, with a ratio of high to low photon flux of 100. The transfer function was adapted for the-loop frame for each case, and the range was 140–1054 Hz. The agreement is remarkable, even for a low light level.

B. Compensating the Contribution of the Wavefront Sensor Spatial Aliasing

The three last terms on the right member of Eq. (13) show the contribution of the WFS spatial aliasing that we need to remove from the DM command covariance,

$$\text{alias cov.} = \langle \mathbf{a}_\parallel^\perp \cdot \mathbf{a}_\parallel^{\perp t} \rangle + \langle \mathbf{a}_\parallel \cdot \mathbf{a}_\parallel^{\perp t} \rangle + \langle \mathbf{a}_\parallel^\perp \cdot \mathbf{a}_\parallel^t \rangle. \qquad (24)$$

We can think of two methods to estimate this term. The first would be the procedure proposed in Kolb *et al.* [6], where they propose to run a first w_0 and L_0 estimate ignoring the aliasing term, then use a model of the aliasing term adjusted for the seeing amplitude and do a second estimation taking into account the aliasing term. According to Kolb *et al.* this technique quickly converges and produces good results.

We think it is not necessary to apply an iterative procedure. Indeed, the effect of aliasing is to systematically increase the DM command variance in relation to the number of lenslets
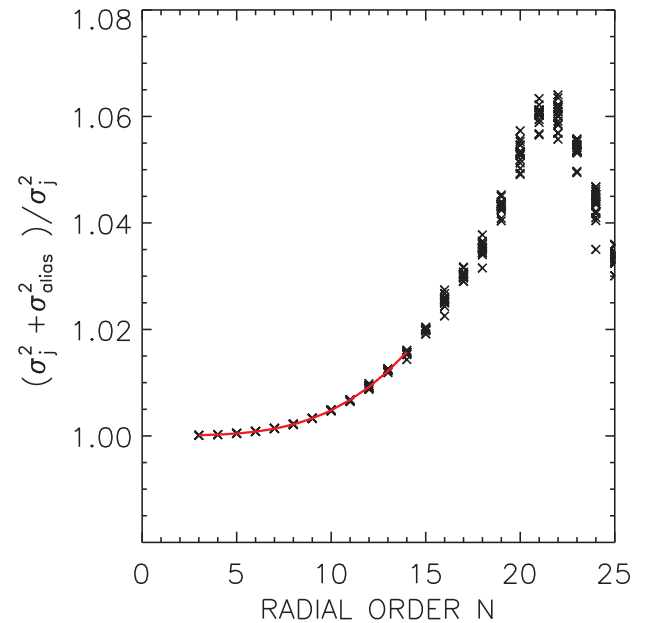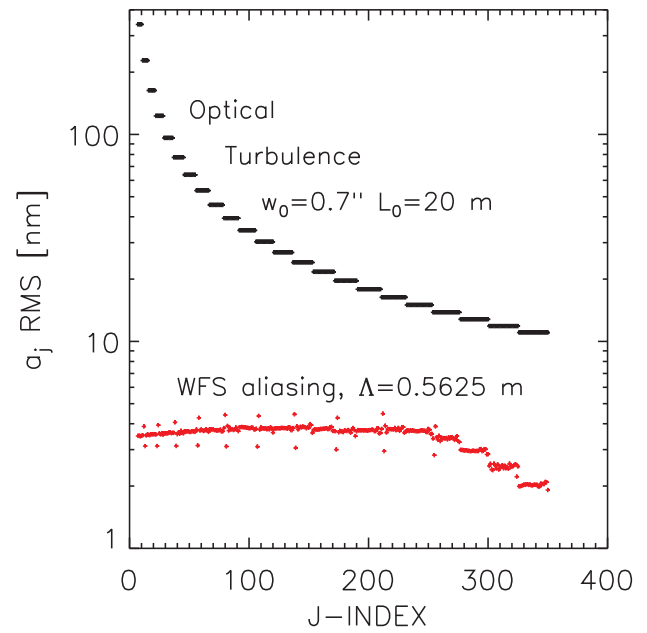

Fig. 14. Top, Zernike coefficient variance for seeing and WFS aliasing. Bottom, relative excess of Zernike coefficient variance due to aliasing for the Keck AO WFS.

or degree-of-freedom of the WFS, independently of the seeing amplitude. Thus, because this effect is systematic, we can compute numerically, using a Monte Carlo procedure, the variance of the WFS aliasing expressed in the modified Zernike coefficients for $D/r_0 = 1$, and simply compensate the Zernike variances for this factor.

Figure 14, top, shows the RMS of the aliasing Zernike coefficients and the RMS of the OT Zernike coefficients for a seeing of 0.7′′, 20 m outer scale, and the Keck AO system DM pitch. The computation is based on the generation of random phase screens drawn from the aliasing spatial power spectrum

given in Jolissaint [17]. These phase screens are then projected in the modified Zernike basis. The top figure shows that the aliasing RMS is quite constant over a large range of indexes until it drops. Therefore, as the OT Zernike variance decreases steeply with j, the relative effect of aliasing increases towards the high orders until a maximum is reached (bottom of Fig. 14). We have computed the latter curve for different values of the outer scale (down to 10 m) and saw essentially no change.

Therefore, it is possible to build an empirical model of the variance excess as a function of the radial order, and compensate this excess on the modified Zernike variance after the noise has been compensated. Our model is an order 4 polynomial, fit to the curve shown in Fig. 14, valid for the range $n = 3$ to $n = 15$:

$$\eta_n = p_0 + p_1 n + p_2 n^2 + p_3 n^3 + p_4 n^4, \quad (25)$$

with

$$\mathbf{p} = [0.998935, 7.706682 \times 10^{-4}, -1.823336 \times 10^{-4},$$
$$1.903760 \times 10^{-5}, -2.762067 \times 10^{-7}].$$

We have found that the impact of the aliasing error is minor, only about 0.4% excess of seeing angle. But again, as our objective is to compensate all possible sources of systematic errors, we did implement this correction in our algorithm.

7. ON-SKY VALIDATION

The PSF-R project at Keck Observatory started in 2007 with Flicker [18], and was continued and completed by our team from 2009 to 2017. During this period, more than 1000 AO runs were dedicated to the project and 841 were considered valid to test our PSF-R algorithm. Of these, 636 runs are in NGS mode and 205 in LGS mode. There is no conceptual difference between the two modes as far as seeing estimation is concerned. In reality, a close inspection of the modified Zernike coefficient variances showed some unexpected behavior in the LGS case, requiring further rejection of some modes. At the end, the seeing estimation quality is no different for the two modes.

In this section, after a summary of the OT estimation procedure, we will show how well the variance model we developed fits the data, and then show a comparison of the estimated seeing with a simultaneous seeing estimated from on-loop PSF on the same telescope, as well as with differential image motion monitor (DIMM) and multi-aperture scintillation sensor (MASS) seeing measurements.

A. Calculating the Seeing Angle and Outer Scale, in Practice

The procedure to get the seeing angle and the outer scale from the raw DM commands is summarized as follows:

1. Identify and discard the bad modes by inspection of the modified Zernike variances for a significant number of AO experiments. This point is very critical and requires some analysis of the system's behavior;

2. Remove the average from the DM commands in case an offset is applied on the DM to compensate for nonturbulent static aberrations. Optical turbulence wavefront error shall be null on average;

3. Compute the DM command covariance $\langle \mathbf{mm}^t \rangle$;

4. Estimate the DM command noise covariance $\langle \mathbf{nn}^t \rangle$ and subtract it from the DM command covariance;

5. Transform the noise-free DM command covariance into the modified Zernike coefficient covariance matrix;

6. Remove the bad modes from the modified Zernike covariance matrix;

7. Keep only the *variances* of the modified Zernike coefficients; indeed it makes enough valid data points, and in any case the outer-scale damping model is only for the variances;

8. Apply the aliasing correction factor to the modified Zernike variances;

9. Construct the normalized variance model, i.e., for $D/r_0 = 1$ and an infinite outer scale;

10. Divide the modified Zernike variances by the normalized model for each mode individually;

11. Find the ratio D/L_0, making the preceding ratio independent of the j-index, using the empirical model for the outer-scale damping $\mathcal{W}_{j,j}$; this provides the best estimation of the outer scale;

12. Divide once again the modified Zernike variances by the normalized model for each mode individually, but now including the outer-scale damping; we get, for each good mode, a value of the $(D/r_0)^{5/3}$ ratio from which we extract a series of r_0 values, and then the average r_0 and w_0 for the AO run, as well as an estimate of the uncertainty on r_0, given by

$$\sigma(r_0) = 0.6 D \langle (D/r_0)^{5/3} \rangle^{-8/5} \sigma[(D/r_0)^{5/3}]; \quad (26)$$

13. As a verification, find the $(D/r_0)^{5/3}$ ratio that minimizes the total quadratic difference between the variances and the model, including the effect of the outer scale; in principle, this best fit $(D/r_0)^{5/3}$ should be compatible with the average value computed from individual modes, i.e., it must be within the 1-σ dispersion range; if not, it is a sign that there might be an issue with the data.

B. Comparison of the Variance Model and the Measured Variances in NGS Mode

The estimation of w_0 and L_0 are made via a fit of the modified Zernike variance model to the DM command variances. Therefore, it is critical to verify how well the model represents the real data. In order to do this, we normalized the variances by the factor $(D/r_0)^{5/3} \mathcal{W}_{j,j}(D/L_0)$, using for each set the Fried parameter and outer scale determined from the set itself. Figure 15 shows the comparison of the model variances, in green and black, and the average variances for the 636 NGS cases. From this, we concluded the following:

• The model is consistent with the data on average (see in particular the zoomed graph). The 1-σ error bars almost always include the model prediction except for the modes for which the azimuthal index $m = 1$, where the model is strangely almost two orders of magnitude above the data. We were not able to identify the origin of the discrepancy, and we simply considered all $m = 1$ modes as bad modes, excluded from the fit. The purely radial modes, $m = 0$, while compatible with the data, showed also a systematic trend; because we had so many valid modes, we decided to also discard these modes in order not to add a possible systematic error.

• Beyond the j-index 120, we found that the difference between the model and the average variance was getting gradually larger than the σ of the variances (not for all the modes,
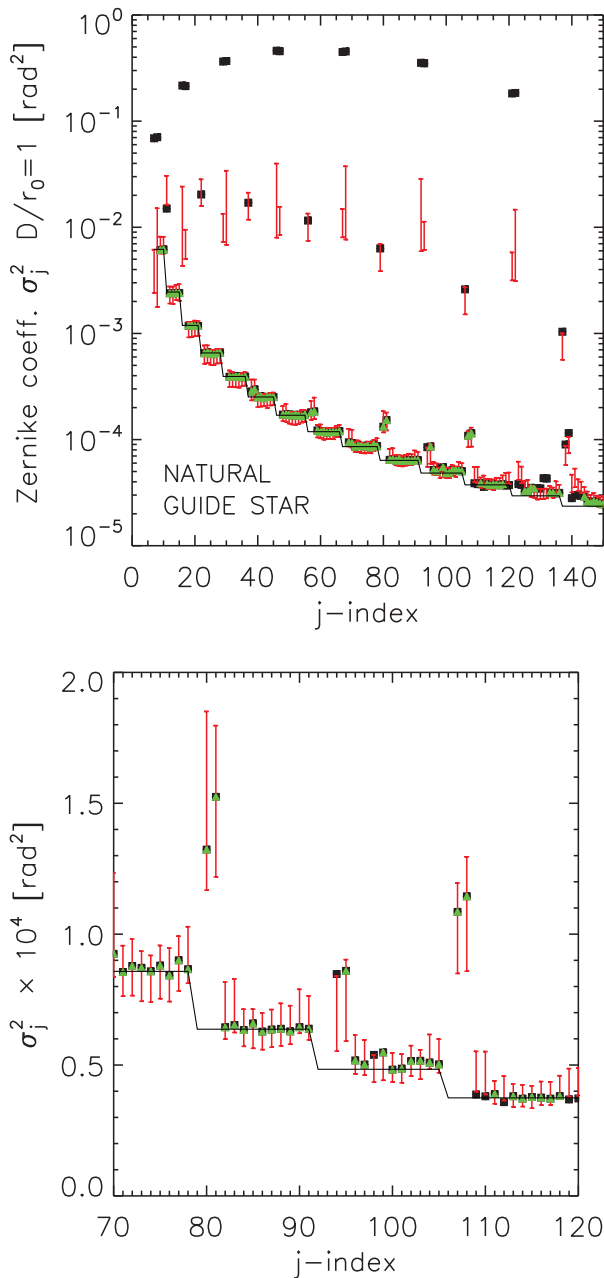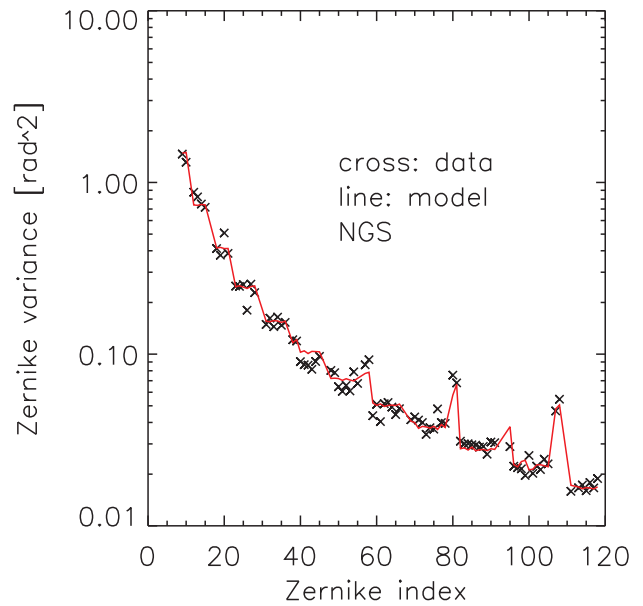
Fig. 16. Example of model fitting to telemetry data. Case August 1st, 2013, data set 0004. Seeing was $0.44'' \pm 0.03''$ (1-σ) and the outer scale 12 m. Only the good modes were used for the model fit.

are identified, it should be safe to use the simpler Noll model, with Winker factor, for the fit.

Figure 16 shows an example of model fitting to the data after final selection of the good modes. There is some statistical noise, certainly due to the fact that the AO run exposures were limited in time: indeed, only a stationary optical turbulence and an infinite exposure time would make the measurements perfectly identical to the OT models we are using. Overall, though, the model matches the data because the residual statistical error due to the limited exposure time has a random sign for each mode, and gets somewhat cancelled in the fitting process.

It is important to note here that because the seeing changes relatively rapidly, the seeing we are estimating can only be an average of the seeing during the AO run science exposure. If the seeing has changed too much, i.e., if the turbulence has been too unstable during the AO run, there will be an excess variance in the DM data with respect to the model we use. This is clearly a limit of the current method, which assumes spatial and temporal stationarity of OT. We have been made aware that techniques to extract the OT parameters for a non-stationary turbulence have been developed (see Brennan and Mann [19] and references therein). Implementation of these techniques in the context of astronomical AO application is left to another study.

C. Comparison of the Variance Model and the Measured Variances in LGS Mode

Figure 17 shows the comparison of the variance model and the average variance in LGS mode for the 205 sets. Overall, the match between the model and the data is good, and the same comments as for the NGS mode apply except for one thing: for all the Zernike polynomials whose azimuthal component is in $\cos m\theta$, with m even, there is a systematic excess of variance as
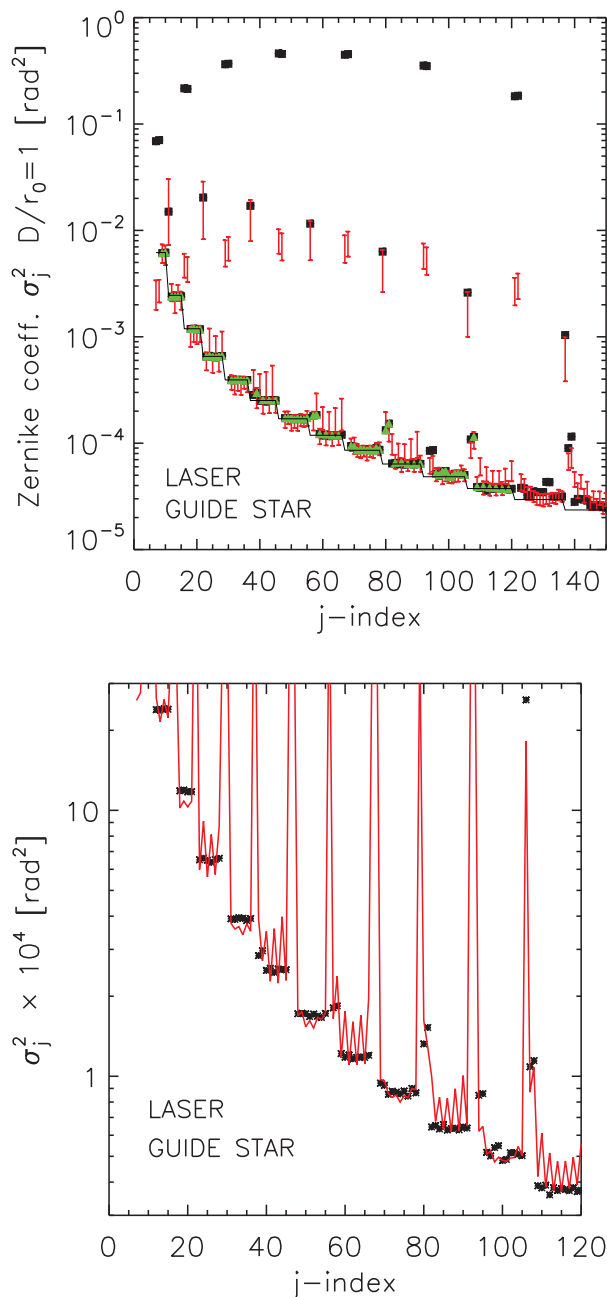
Fig. 15. NGS mode. Top figure: average of the variances of the modified Zernike coefficients calculated from the DM actuator commands, with 1-σ bars, in red. In green, model prediction of the variances for the good modes. For each AO run, and the model, we have normalized the variances by the ratio $(D/r_0)^{5/3}$ and removed the effect of the outer scale by dividing by the Winker's factor, using the value of L_0 assessed from the data. In black, the same for the modes $m = 0$ (first sets of points above the green line) and $m = 1$ (top series of points). Bottom: a zoom in the region $j = 70$–120.

though), so we decided to reject the modes $j > 120$ as well. Overall, we were left with 90 valid modes in NGS mode, in the range $j = 9$ to $j = 120$.

• For a significant fraction of the modes, Noll's model is perfectly suitable, i.e., the representation and sampling errors do not affect the quality of the model. Once these modes

the NGS and LGS the same way. It should therefore come from the LGS data itself. Keck AO is a zonal system, so we cannot expect the actuator control itself to be at the origin of this asymmetry.

The objective of the seeing estimation project is not to debug the AO system, however, so therefore we simply decided to discard the Zernike modes impacted by this effect. We were therefore left with 75 good LGS modes, still enough for an accurate determination of OT. Note that before suppressing these modes, the estimated seeing in LGS mode was systematically about 15% higher than in NGS mode. This example shows the importance of a close inspection of the system behavior in order to avoid spurious systematic errors in the seeing determination.

D. WFS Noise and Error in the Seeing Determination

If the noise contribution to the variance has been well subtracted, then there should be no correlation between the WFS noise level and the error in the seeing angle. Figure 18 shows that such is indeed the case for both NGS and LGS, for all 841 data sets. The noise variance in LGS mode is simply higher than in NGS mode, but there is no correlation with the relative error in the seeing angle.

E. Seeing Angle and Outer-Scale Statistics

We show in Figs. 19 and 20 the seeing angle and outer-scale distribution for all the 841 valid measurements done during the PSF-R project. The mean and median seeing are in line with the values measured for this site, albeit slightly larger. This might be due to some mirror seeing on the telescope. According to Zago [20], what is called dome seeing is actually essentially coming from a temperature difference between the primary mirror and the immediate layer or air above it. The rule of thumb, validated on many telescopes, is that a difference of
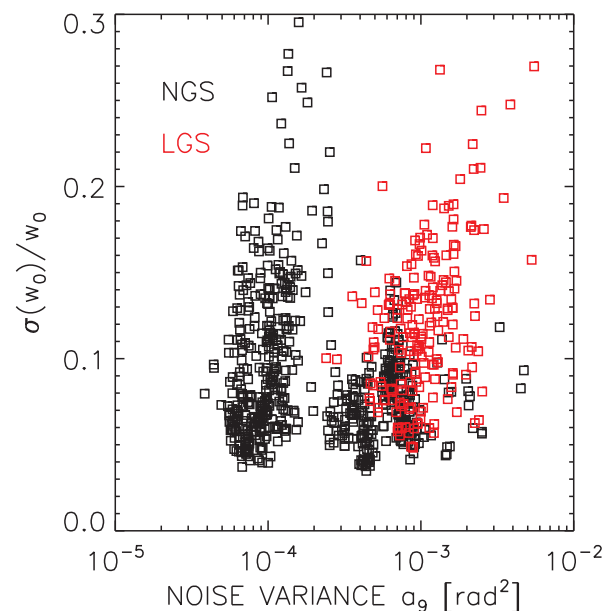
Fig. 17. LGS mode. Top figure: average of the variances of the modified Zernike coefficient variances calculated from the DM actuator commands, with 1-σ bars, in red. In green, model prediction of the variances for the good modes. For each AO run and the model, we have normalized the variances by the ratio $(D/r_0)^{5/3}$ and removed the effect of the outer scale by dividing by the Winker's factor using the value of L_0 assessed from the data. In black, the same for the modes $m = 0$ (first sets of points above the green line) and $m = 1$ (top series of points). Bottom: a zoom in the σ_j^2 region around 10^{-4} rad^2 showing an unexpected oscillation of the variances for the even azimuthal modes.

Fig. 18. Relative uncertainty of the seeing angle determination as a function of the variance of the noise for modified Zernike coefficient a_9 (considered as a proxy for the noise variance). In black, NGS cases; in red, LGS case.

shown in Fig. 17, bottom. This behavior is not seen at all in NGS mode. Thus, there is some systematic error in LGS mode whose origin we have not been able to identify. We do not think it is coming from the data processing, as we process
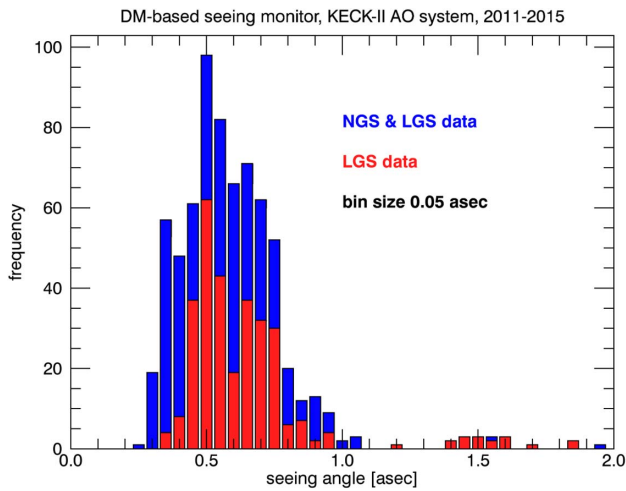
Fig. 19. Histogram of the seeing measurements in NGS and LGS modes for the 841 experiments. Median seeing 0.62, mean seeing 0.70, standard deviation 0.3.

+1°C between the air and the mirror generates 0.1″ of seeing. We also see that there is no statistical difference between the results obtained in NGS and LGS mode. Note that the uncertainty on the seeing (1σ) for each measurement was 0.03″ on average.

The outer scale we are measuring is on average a factor 2 smaller than values measured on the same summit on a nearby 8 meter telescope (Subaru) by the RAVEN AO system team (Ono et al. [21]) on different nights (which might also explain some part of the observed discrepancy). Using a SLODAR technique, they were able to retrieve vertical profiles of the outer scale and show that this parameter varies significantly with the altitude in a range 15–35 m, on average. The SLODAR technique, as it makes use of the correlation of the slopes from an array of Shack–Hartmann lenslets, is in principle relatively insensitive to the limited size of the telescope aperture while, in the DM-seeing method, we determine the
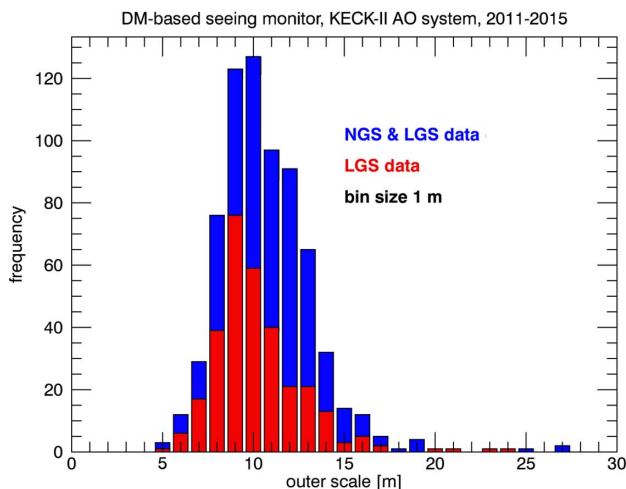

Fig. 20. Histogram of the outer-scale measurements in NGS and LGS modes for the 841 experiments. Median 12 m, mean 12.7 m, standard deviation 6 m.

outer scale from the effect it has on the Zernike modes variances over the full aperture. Therefore, our outer-scale determination method critically depends on the pupil diameter, and it might be that the SLODAR and DM-seeing methods do not measure the outer scale with the same biases. This assumption remains to be explored.

We tried to *force* the outer scale to 20 m in the data reduction, but found that the fitting of the model with the low-order variances was not satisfactory, with a model variance always larger than the measurements at low order. As a consequence, the estimated seeing angle was lowered by about 5%.

In our opinion, here we are reaching the limits of the optical turbulence theory. The assumption that the turbulent flow is homogeneous and the scales of the eddies distributed according to the Kolmogorov law (see Tatarski for details) is truly valid in the free atmosphere, but ground structures like the observatory building and dome certainly break the homogeneity of the flow, where optical turbulence is at its strongest. Also, if the turbulence is at its strongest—near the ground and the dome slit— where the outer scale is at its lowest, it should not be a surprise that the outer scale measured on the *full aperture* tends to be equal to the slit and mirror diameter (see Eq. 12 in Ono et al., showing how the optical outer scale is weighted by the optical turbulence profile). This is of course only an assumption needing further exploration as well.

Besides, we must not forget, as Voitsekhovich and Cuevas [22] remind us, that the von Karman model of the turbulent phase spatial power spectrum, at the basis of all models used so far to account for the damping effect of the outer scale, is *only* a simple *empirical model* not based on physics. In fact, other models exist that produce, according to Voitsekhovich, similar results as the VK model.

What we can finally conclude from our measurements is that there is a significant damping of the low-order aberration variances with respect to a fully developed Kolmogorov flow, and that this damping is relatively well described by the von Karman empirical modification of the Kolmogorov model using an outer scale of 13 m on average. Deciding if the VK model is appropriate or not to describe the real shape of the turbulent flow near the telescope aperture, or if a more sophisticated inhomogeneous model shall be used, is beyond the scope of this work.

F. Note on the Number of Good Modes and the Seeing Determination Accuracy

The selection of the first good mode has an impact on the accuracy with which the outer scale is estimated: the lower the j-index, the stronger the L_0-damping effect and therefore the better the accuracy on L_0, which has an immediate impact on the seeing determination (ignoring the problem with the potential instrument aberrations); on the other hand, the higher the last j-index, the more data points we have and the better the seeing estimation, but we also need to remove bad modes here and there for various reasons. As we have seen, we are left with 90 data points in NGS mode and 75 in LGS mode. In principle, as we have de-trended the measured variance from the outer-scale damping, when we divide the variances with Noll's model, we should see a straight line. The average of this line gives the mean $(D/r0)^{5/3}$, from which we get r_0 and the

seeing. As the departure from Noll's model has many different (unknown) origins, we expect the error distribution to be Gaussian, so the RMS on the mean r_0 shall be given by the classical formula $\sigma(\text{mean}) = \text{mean}(\sigma(\text{data}))/\sqrt{\text{nb.data}}$. So, going from 90 to 75 data points (NGS to LGS), the relative loss is 10%, i.e., the statistical error of the seeing determination from the LGS data is only 10% larger than that for the NGS case.

But all this is relatively theoretical. Indeed, in our understanding, the accuracy of the OT parameters has more to do with the selection of the good modes than with the number of modes, assuming of course that there are enough valid modes. As we see in the Keck example, a few tens of modes well distributed from the very first to last mode shall be enough. For any other system, we would therefore recommend carefully examining the behavior of the modal variances to select the appropriate modes. Also, the only solid way to estimate the accuracy of the seeing determination is to run a AO on/off experiment as we describe next.

G. Comparison with Open-Loop PSF Seeing

Certainly the most important test of our method was the direct comparison of the DM-monitor seeing with the seeing extracted from simultaneous on-sky open-loop PSF, acquired on the same telescope, on the same optical axis. In such a case, it is expected that both seeings should be highly correlated. During two nights, June 22 and 23 of 2011, we did 96 AO runs alternated with 75 open-loop PSF acquisitions. The typical delay between a closed-loop and an open-loop run was 90 s. This delay was too long to catch the same turbulent conditions, but short enough to catch the long term evolution of the atmosphere over a few minutes, and verify that the seeing evolution were identical in both time series (Fig. 21).

On the Keck AO system, the open-loop mode is actually a tip-tilt correction mode, so the seeing cannot be estimated directly from the long exposure PSF themselves. Furthermore, there is the PSF improvement due to the outer scale. We therefore built, using a Monte Carlo simulation of tip-tilt correction, a library of synthetic long exposure tip-tilt corrected PSF, for a range of seeing values from 0.2″ to 1.9″, and an outer scale equal to the average we have measured in our data set, 12 m. Then, after careful cosmetic cleaning of the sky open-loop PSF (acquired with the near infrared camera NIRC2, at 1.65 μm) we looked into the library for the PSF whose Strehl ratio was the closest to the sky PSF Strehl. We knew that there were some uncorrected static aberrations in the system (about 150 nm), but their contribution on the tip-tilt corrected PSF Strehl was negligible.

The median rate of change of the seeing during the experiments was, measured from the seeing time series themselves, 0.3 mas/s, in both directions (increase or decrease of the seeing). Therefore, the seeing change from a closed-loop to an open-loop run, separated by 90 s, was on average ±0.03″. Adding to this the uncertainty of 0.03″ of the seeing angle, we end up with a probable deviation of ±0.06″ between a DM-based seeing measurement and the subsequent PSF-based seeing measurement. In Figs. 21, we show the superposed time evolution of the DM- and PSF-based seeing measurements for the two on-sky experiments of June 22 and 23, 2011. Most of
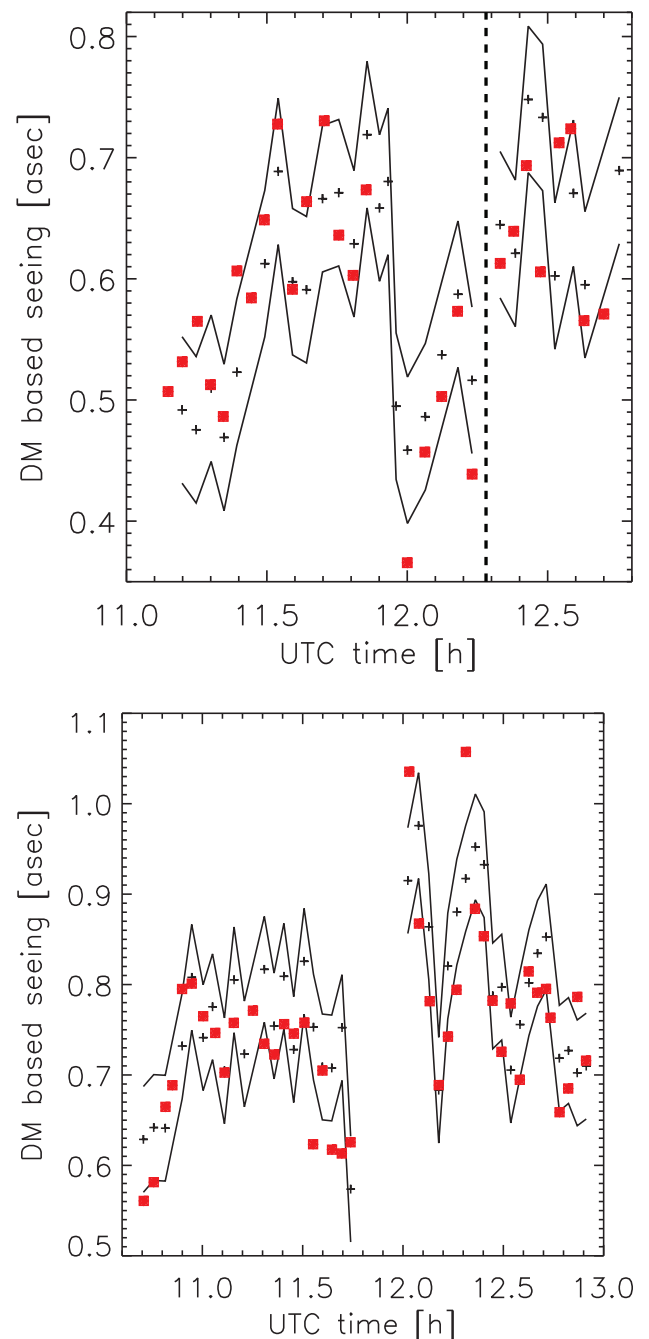

Fig. 21. Closed-/open-loop seeing experiment. June 22/23, 2011 (top/bottom). Plus signs, DM-seeing; red squares, PSF seeing. The continuous lines show the range of values within which the PSF seeing is expected, if the PSF seeing is the same as the DM-based seeing. The dashed vertical line indicates an interruption in the data acquisition for about 10 min.

the PSF seeing is within the expected range, so we can conclude that the two series are compatible, which is also apparent in their statistics, given in Table 2.

We show the correlation between the DM and PSF seeing measurements in Fig. 22, where the DM-based seeing measurements has been interpolated at the same time as the PSF measurements. The correlation coefficient is 90.6% and the

Table 2.   Statistics of the DM- and PSF-Based Seeing Measurements for June 22 and 23, 2011

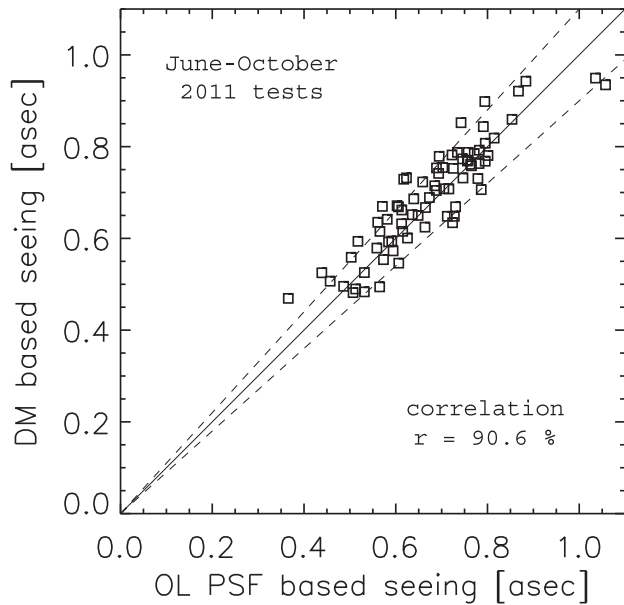|	June 22		June 23	
	DM	**PSF**	**DM**	**PSF**
$\langle w_0 \rangle$	0.59″	0.59″	0.78″	0.75″
σw_0	0.09″	0.09″	0.11″	0.10″

Fig. 22.   DM seeing and PSF seeing for the two nights all together, plus five data points taken on October 13, 2011. The DM seeing values are an interpolation at the time of the PSF seeing acquisition. The dashed lines show a range of ±10% from the PSF seeing reference.

slope between the two series is 1.02. Most of the DM-based seeing values are within ±10% of the PSF-based values. In our opinion, these results fully validate the DM-seeing monitor technique.

H. Comparison with DIMM and MASS Seeing

The last test we did was comparing the DM-based seeing with simultaneous measurements made by the Mauna Kea seeing monitors' *differential image motion monitor* (DIMM, Sarazin and Roddier [23]) and *multi aperture scintillation sensor* (MASS, Kornilov *et al.* [24]). The DIMM and MASS data are taken from the Mauna Kea Weather Center web site archive (http://mkwc.ifa.hawaii.edu/current/seeing/). Figure 23 shows the night average seeing for the DM/DIMM/MASS monitors for nine nights between June 2011 and July 2015.

It appears that for most of the nights, the DM and DIMM night average seeing are similar. This is not the case for the MASS seeing, which is for five over eight nights significantly smaller than the DM values, but this is expected, as it is known that the MASS monitor is not sensitive to the low-altitude layers. These measurements can be interpreted as an indication that most of the time there is a significant ground layer of optical turbulence at Mauna Kea, a fact that is well known (see for instance Ono *et al.* [21] and reference herein).
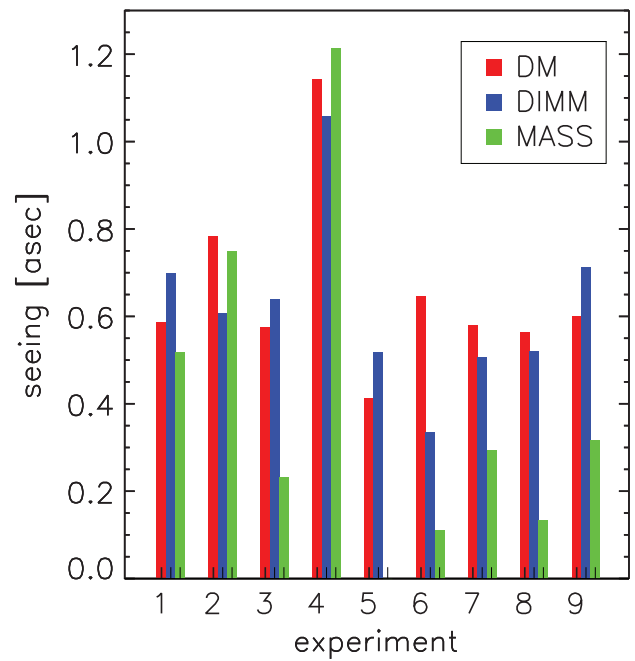

Fig. 23.   Average seeing during the same period of time as the AO runs, for nine nights. Dates and seeing values are given in Table 3. MASS data is missing for night # 5.

Table 3.   Mean Seeing Measured with the DM, PSF, DIMM, and MASS for the Nine Dates Indicated[a]

Exp	Date	DM	PSF	DIMM	MASS
1	2011/06/22	0.59	0.59	0.70	0.52
2	2011/06/23	0.78	0.75	0.61	0.75
3	2011/10/13	0.58	0.56	0.64	0.23
4	2012/02/10	1.14	–	1.06	1.22
5	2013/02/03	0.41	–	0.52	–
6	2013/09/14	0.65	–	0.34	0.11
7	2014/07/11	0.58	–	0.51	0.29
8	2015/03/31	0.56	–	0.52	0.13
9	2015/07/01	0.60	–	0.71	0.32

[a]Unit is asec.—means data is not available.

That being said, while the correlation between the nightly average can be relatively good, at least with the DIMM values, this is not the case on a shorter time basis (minutes/hours). This is demonstrated by the RMS of the difference between the DM, DIMM, and MASS seeing shown in Table 4: the DIMM-DM dispersion is four times larger than the open-loop PSF-DM dispersion, and the MASS-DM one is six times larger.

Also, there can be important differences between the DM, DIMM, and MASS seeing from one night to another as well as

Table 4.   Average Dispersion Between DM Seeing and the Other Sensors[a]

OL-PSF	DIMM	MASS
0.06″	0.22″	0.37″

[a]The DIMM and MASS seeing were interpolated at the time of the DM-seeing acquisition.
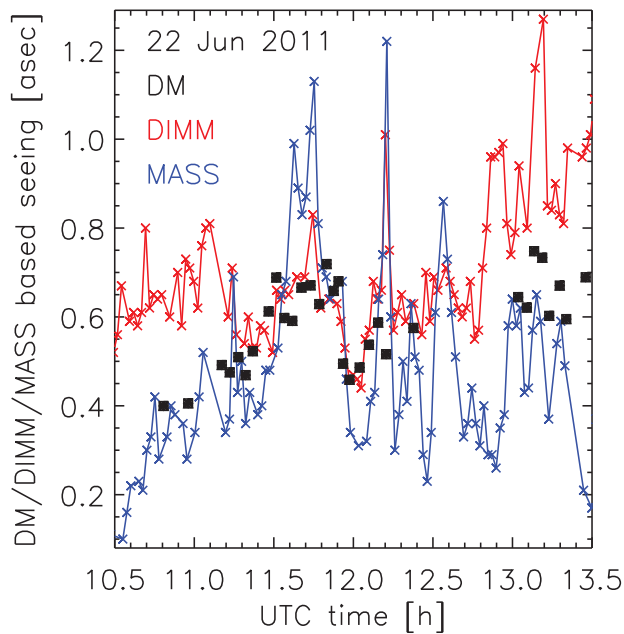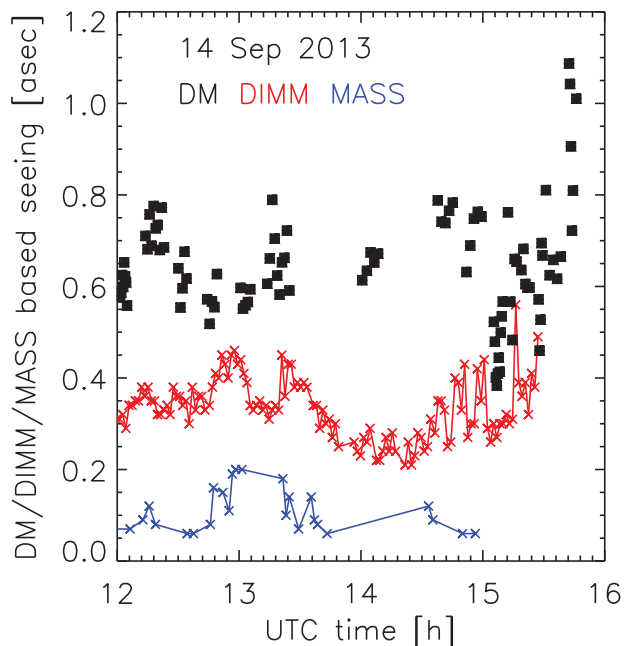
Fig. 24. Comparison of the DIMM, MASS, and DM seeing for the night of June 22/23, 2011, when correlation of the night average was at its highest amongst our data sets.

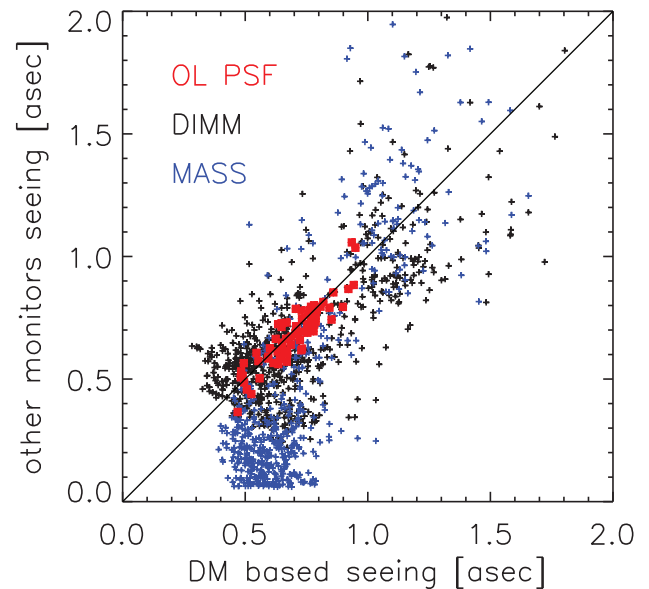**Fig. 26.** Comparison of the DIMM, MASS, OL PSF, and DM seeing. The DIMM/MASS seeing was interpolated at the time of the DM seeing acquisition.

during a given night. The night of June 22, 2011 (Fig. 24) shows a case in which the average seeing was relatively similar, but we can see that this correlation was *mostly coincidental*. The night of September 14, 2013 (Fig. 25) shows an example where the three monitors were producing totally different results.

Figure 26 shows the DIMM, MASS, and OL PSF seeing versus the DM seeing. It is obvious that the OL PSF seeing is

much more correlated with the DM seeing than are the DIMM and MASS seeing. This is a clear demonstration of the fact that the seeing changes significantly from a place to another because of the influence of the ground structures on the turbulent flow, which might change with the wind direction, and because the monitors are not sensing the turbulence from the same altitude. Besides, mirror seeing can be present.

As a consequence, we think that an accurate estimation of the seeing associated with a given AO observation requires a measurement collocated with the system optical axis at the same time as the observation. The DM-seeing monitor is the ideal solution for this. A distant seeing monitor cannot produce any useful results in that respect, and shall only be used for site monitoring. *It might even be that, because of the poor correlation between seeing monitors and the telescope seeing measured by the DM seeing, observation scheduling based on seeing prediction would only have a limited interest* unless the very local and mirror seeing could be predicted. It is therefore essential, in our understanding, to collocate as much as possible the OT monitors and the optical axis of the telescope.

8. CONCLUSIONS

We have presented a detailed analysis of the systematic and random errors affecting the determination of the seeing angle and outer scale of optical turbulence from the deformable mirror commands of an adaptive optics system. Mitigation or correction solutions have been proposed for each term. The method was developed for both the natural and laser guide star modes of the adaptive optics system of the W. M. Keck-II telescope, and can be applied to any other system. The method has been validated with a comparison to simultaneous measurements of the seeing from open-loop PSF acquired on the same optical axis. We have demonstrated that an accuracy of 10% on the determination of the local and instantaneous seeing is achievable.

Fig. 25. Comparison of the DIMM, MASS, and DM seeing for the night of September 14/15, 2013, when correlation of the night average was at its lowest.

We tested the DM wavefront for stationarity in the pupil, a particularly important requirement in this method, and showed that the pupil edges had to be avoided by selecting an annulus inside the telescope pupil for the seeing determination. Zernike projection error on the DM influence function basis and numerical representation error have been identified and compensated by a proper use of a modified Zernike polynomial basis. A noise covariance determination from the power spectrum of the actuator commands has been developed, and comparison of the noise amplitude with the expected behavior as a function of the number of photons per integration time has validated the approach. A simple method to compensate for wavefront sensor aliasing has been developed.

The statistical analysis of the DM commands expressed in the modified Zernike basis demonstrates the validity of the Kolmogorov model, with the von Karman empirical modification, to describe the Keck AO system behavior. This in turn indicates that, by using this system, it is possible to extract the OT parameters from the telemetry (which is not the case on all systems) because non-Kolmogorov sources of dynamical errors are negligible. That being said, in LGS mode, an unexpected excess of dynamical aberration was identified for modes with an even azimuthal order m. These modes were simply discarded from the seeing determination process. After this correction, no statistical difference between the natural and laser guide star modes was found.

The statistics of the seeing angle determined for 841 AO runs from 2011 to 2015 is similar to the expected value for the Mauna Kea summit, about $0.6''$. The estimated outer scale is smaller than the average value measured with other monitors. We postulate without proof that this might be due to the difference between the geometry of the outer-scale determination in the DM-seeing approach, where the whole pupil is used, and the other methods, which study the statistics of the wavefront as a function of the separation vector within the pupil. The dome structure might also have an influence.

We finally demonstrated that the DM-based seeing was highly correlated with the seeing measured on the same axis, at a quasi-simultaneous time, on open-loop PSF. The relative difference was 10% on average, with a dispersion of only $0.06''$. This method is therefore valid for retrieving accurate seeing determination values, a particularly critical aspect for system performance validation and other sensitive post-AO methods such as PSF reconstruction. On the contrary, the difference between the DM and DIMM seeing can be more than 40%, and more than 80% with the MASS seeing. It is therefore highly recommended not to use non-collocated seeing monitors when accurate seeing estimation is required at a given telescope.

REFERENCES

1. F. Rigaut, G. Rousset, P. Kern, J.-C. Fontanella, J.-P. Gaffard, F. Merkle, and P. Léna, "Adaptive optics on a 3.6-m telescope—results and performance," Astron. Astrophys. **250**, 280–290 (1991).
2. J.-P. Véran, F. Rigaut, H. Maître, and D. Rouan, "Estimation of the adaptive optics long-exposure point spread function using control loop data," J. Opt. Soc. Am. A **14**, 3057–3069 (1997).
3. J. R. Lu, A. M. Ghez, S. Yelda, T. Do, W. Clarkson, N. McCrady, and M. Morris, "Recent results and perspectives for precision astrometry and photometry with adaptive optics," Proc. SPIE **7736**, 77361I (2010).
4. M. Schöck, D. Le Mignant, G. A. Chanan, P. L. Wizinowich, and M. A. van Dam, "Atmospheric turbulence characterization with the Keck adaptive optics systems. I. Open-loop data," Appl. Opt. **42**, 3705–3720 (2003).
5. T. Fusco, G. Rousset, D. Rabaud, E. Gendron, D. Mouillet, F. Lacombe, G. Zins, P.-Y. Madec, A.-M. Lagrange, J. Charton, D. Rouan, N. Hubin, and N. Ageorges, "NAOS on-line characterization of turbulence parameters and adaptive optics performance," J. Opt. A **6**, 585–596 (2004).
6. J. Kolb, N. Muller, E. Aller-Carpentier, P. Andrade, and J. Girard, "What can be retrieved from adaptive optics real-time data?" Proc. SPIE **8447**, 84475U (2012).
7. V. Tatarski, *Wave Propagation in a Turbulent Medium* (Dover, 1961), translated by R. A. Silverman.
8. F. Roddier, "The effect of atmospheric turbulence in optical astronomy," in *Progress in Optics*, E. Wolf, ed. (North-Holland, 1981), Vol. **XIX**, pp. 281–376.
9. D. L. Fried, "Optical resolution through a randomly inhomogeneous medium for very long and very short exposures," J. Opt. Soc. Am. **56**, 1372–1379 (1966).
10. C. E. Coulman, "Fundamental and applied aspects of astronomical seeing," Appl. Opt. **23**, 19–57 (1985).
11. R. Conan, R. Avila, L. J. Sánchez, A. Ziad, F. Martin, J. Borgnino, O. Harris, S. I. González, R. Michel, and D. Hiriart, "Wavefront outer scale and seeing measurements at San Pedro Mártir observatory," Astron. Astrophys. **396**, 723–730 (2002).
12. A. Ziad, J. Maire, J. Borgnino, W. Dali Ali, A. Berdja, K. Ben Abdallah, F. Martin, and M. Sarazin, "MOSP: monitor of outer scale profile," in *Adaptative Optics for Extremely Large Telescopes (AO4ELT-I)*, 2010.
13. R. J. Noll, "Zernike polynomials and atmospheric turbulence," J. Opt. Soc. Am. **66**, 207–211 (1976).
14. D. M. Winker, "Effect of a finite outer scale on the Zernike decomposition of atmospheric optical turbulence," J. Opt. Soc. Am. A **8**, 1568–1573 (1991).
15. L. Jolissaint, J.-P. Veran, and J. Marino, "OPERA, an automatic PSF reconstruction software for Shack-Hartmann AO systems: application to Altair," Proc. SPIE **5490**, 151–163 (2004).
16. M. A. van Dam, A. H. Bouchez, D. Le Mignant, E. M. Johansson, P. L. Wizinowich, R. D. Campbell, J. C. Y. Chin, S. K. Hartman, R. E. Lafon, P. J. Stomski, Jr., and D. M. Summers, "The W. M. Keck observatory

laser guide star adaptive optics system: performance characterization," Publ. Astron. Soc. Pac. **118**, 310–318 (2006).

17. L. Jolissaint, "Synthetic modeling of astronomical closed loop adaptive optics," J. Eur. Opt. Soc. Rapid Publ. **5**, 10055 (2010).

18. R. Flicker, 2008, https://www.lao.ucolick.org/static/PsfReconstruction/psf_rev.pdf.

19. T.-J. Brennan and D. C. Mann, "Estimation of optical turbulence characteristics from Shack Hartmann wavefront sensor measurements," Proc. SPIE **7816**, 781602 (2010).

20. L. Zago, "Engineering handbook for local and dome seeing," Proc. SPIE **2871**, 726–736 (1997).

21. Y. H. Ono, C. M. Correia, D. R. Andersen, O. Lardière, S. Oya, M. Akiyama, K. Jackson, and C. Bradley, "Statistics of turbulence parameters at Mauna Kea using the multiple wavefront sensor data of RAVEN," Mon. Not. R. Astron. Soc. **465**, 4931–4941 (2017).

22. V. V. Voitsekhovich and S. Cuevas, "Adaptive optics and the outer scale of turbulence," J. Opt. Soc. Am. A **12**, 2523–2531 (1995).

23. M. Sarazin and F. Roddier, "The ESO differential image motion monitor," Astron. Astrophys. **227**, 294–300 (1990).

24. V. Kornilov, A. Tokovinin, N. Shatsky, O. Voziakova, S. Potanin, and B. Safonov, "Combined MASS-DIMM instruments for atmospheric turbulence studies," Mon. Not. R. Astron. Soc. **382**, 1268–1278 (2007).